



## Dimensional connectomics of anxious misery, a human connectome study related to human disease: Overview of protocol and data quality

Darsol Seok<sup>a</sup>, Nathan Smyk<sup>a</sup>, Marc Jaskir<sup>a</sup>, Philip Cook<sup>b</sup>, Mark Elliott<sup>b</sup>, Tommaso Girelli<sup>a</sup>, J. Cobb Scott<sup>c</sup>, Nicholas Balderston<sup>a</sup>, Joanne Beer<sup>d</sup>, Janet Stock<sup>a</sup>, Walid Makhoul<sup>a</sup>, Ruben C. Gur<sup>c</sup>, Christos Davatzikos<sup>b</sup>, Russell Shinohara<sup>d</sup>, Yvette Sheline<sup>a,b,c,\*</sup>

<sup>a</sup> Center for Neuromodulation in Depression and Stress, Department of Psychiatry, Perelman School of Medicine, University of Pennsylvania, United States

<sup>b</sup> Department of Radiology, Perelman School of Medicine, University of Pennsylvania, United States

<sup>c</sup> Department of Psychiatry, Perelman School of Medicine, University of Pennsylvania, United States

<sup>d</sup> Penn Statistics in Imaging and Visualization Center, Department of Biostatistics, Epidemiology, and Informatics, Perelman School of Medicine, University of Pennsylvania, United States

### ARTICLE INFO

#### Keywords:

Anxious misery  
Human connectome project  
Brain imaging  
RDoC  
Depression  
Anxiety

### ABSTRACT

Disparate diagnostic categories from the Diagnostic and Statistical Manual of Mental Disorders (DSM), including generalized anxiety disorder, major depressive disorder and post-traumatic stress disorder, share common behavioral and phenomenological dysfunctions. While high levels of comorbidity and common features across these disorders suggest shared mechanisms, past research in psychopathology has largely proceeded based on the syndromal taxonomy established by the DSM rather than on a biologically-informed framework of neural, cognitive and behavioral dysfunctions. In line with the National Institute of Mental Health's Research Domain Criteria (RDoC) framework, we present a Human Connectome Study Related to Human Disease that is intentionally designed to generate and test novel, biologically-motivated dimensions of psychopathology. The Dimensional Connectomics of Anxious Misery study is collecting neuroimaging, cognitive and behavioral data from a heterogeneous population of adults with varying degrees of depression, anxiety and trauma, as well as a set of healthy comparators (to date,  $n = 97$  and  $n = 24$ , respectively). This sample constitutes a dataset uniquely situated to elucidate relationships between brain circuitry and dysfunctions of the Negative Valence construct of the RDoC framework. We present a comprehensive overview of the eligibility criteria, clinical procedures and neuroimaging methods of our project. After describing our protocol, we present group-level activation maps from task fMRI data and independent components maps from resting state data. Finally, using quantitative measures of neuroimaging data quality, we demonstrate excellent data quality relative to a subset of the Human Connectome Project of Young Adults ( $n = 97$ ), as well as comparable profiles of cortical thickness from T1-weighted imaging and generalized fractional anisotropy from diffusion weighted imaging. This manuscript presents results from the first 121 participants of our full target 250 participant dataset, timed with the release of this data to the National Institute of Mental Health Data Archive in fall 2020, with the remaining half of the dataset to be released in 2021.

### 1. Introduction

The term “anxious misery” has gained traction among anxiety and depression researchers (Krueger, 1999; Watson, 2005) and describes over 800 million people worldwide affected by these mental health issues. Diagnostic categories from the Diagnostic and Statistical Manual of Mental Disorders (DSM-5) that fall within the framework of anxious misery include generalized anxiety disorder (GAD), major depressive

disorder (MDD), dysthymic disorder and post-traumatic stress disorder (PTSD) (Watson, 2009). These disorders are not distinct entities, as they frequently co-occur and share important behavioral and phenomenological features, such as increased negative affect (sad mood, negative attentional biases, anxiety), decreased positive affect (anhedonia) and cognitive impairment (dysfunctions in cognitive control, problems with working memory, excessive rumination).

In order to address this overlap in symptoms and underlying

\* Corresponding author at: Richards D307, 3700 Hamilton Walk Philadelphia, Pennsylvania 19104, United States.

E-mail address: [sheline@pennmedicine.upenn.edu](mailto:sheline@pennmedicine.upenn.edu) (Y. Sheline).

<https://doi.org/10.1016/j.nicl.2020.102489>

Received 15 September 2020; Received in revised form 9 October 2020; Accepted 27 October 2020

Available online 3 November 2020

2213-1582/© 2020 Published by Elsevier Inc. This is an open access article under the CC BY-NC-ND license (<http://creativecommons.org/licenses/by-nc-nd/4.0/>).

mechanisms, the Research Domain Criteria (RDoC) project of the National Institute of Mental Health (NIMH) is designed to implement Strategy 1.4 of the NIMH Strategic Plan: “Develop new ways of classifying disorders based on dimensions of observable behaviors and brain functions.” NIMH intends RDoC to serve as a research framework encouraging new approaches for research on mental disorders, in which fundamental dimensions that cut across traditional disorder categories are used as an alternative approach to characterizing patients in clinical studies (Insel, 2014). One of the RDoC domains, the Negative Valence System (NVS), includes the constructs: 1) responses to sustained threat; 2) loss; 3) frustrative non-reward; 4) responses to potential harm; and 5) responses to acute threat. Motivated by this goal, our project, “Functional Connectomics of Anxious Misery” aims to decipher the underlying neurocognitive mechanisms of the NVS by combining high-resolution neuroimaging acquisitions with a comprehensive array of cognitive and behavioral assessments of psychopathology.

Connectivity is a major organizing principle of the nervous system and is fundamental to understanding both brain function and dysfunction (Bressler and Menon, 2010; Friston, 1996). Advances in computation and magnetic resonance imaging (MRI), motivated in part by large efforts such as the Human Connectome Project (HCP; Van Essen et al., 2013), have inspired the generation of novel methods to decipher fundamental aspects of brain organization. By acquiring neural, genetic, neurocognitive and demographic data from hundreds of healthy adults, the HCP has made significant progress towards developing and sharing knowledge about the structural and functional connectivity of the human brain. Further, by establishing standards for data acquisition and image preprocessing, the HCP facilitates the harmonization of data collected from multiple scanners and subject groups. These processes offer the opportunity for analyses that merge data from multiple imaging projects encompassing large sample sizes, a critical requisite for testing and verification of hypotheses in neuroimaging and psychiatry (Van Horn and Toga, 2009).

The current project replicates the same imaging procedures developed for the HCP Lifespan Project (Bookheimer et al., 2019) and adds measures that specifically probe the association of NVS constructs with brain circuits thought to be disrupted in anxious misery disorders. In addition to a suite of neurocognitive measurements standard to the HCP (NIH Toolbox and Penn Computerized Neurocognitive Battery), the present project collected a variety of clinician-administered and self-report instruments that capture a broad spectrum of behavioral and cognitive variability related to anxious and depressive psychopathology. Further, participants performed three separate tasks during their functional MRI scanning session that are relevant to emotional processing, cognitive control and incentive processing. This provides a rich array of important NVS measures to correlate with brain and behavior measures. In addition to a target sample of 200 participants with anxious misery disorders, the Anxious Misery project will enroll 50 healthy participants for comparison and harmonization purposes.

The present article serves as a reference point for researchers interested in using this study’s data. After briefly describing the study’s inclusion criteria and overall study design, this paper will (i) detail the neurocognitive, clinician-administered and self-report instruments given to assess participants’ cognitive and behavioral characteristics, (ii) describe the imaging acquisition protocols, (iii) report descriptive analyses of the imaging data, including structural, functional and diffusion modalities and (iv) report data quality and comparisons of data quality with a representative sample from the HCP Young Adult (HCP-YA) dataset (Van Essen et al., 2013). Our analyses indicate excellent image quality relative to the HCP-YA dataset and neuroimaging profiles that match expected outputs. This manuscript will present results from the first 121 (97 anxious misery, 24 healthy comparators) participants, timed with the projected initial release of these data to the National Institute of Mental Health Data Archive (NDA).

## 2. Study overview

### 2.1. Study sample

To date, this project has collected neuroimaging, clinical and neurocognitive data from 97 participants experiencing symptoms of anxious misery and 24 healthy comparators ( $n = 121$ ) aged 18–60 years (Table 1), education and employment characteristics in Supplementary Table 1), with a target enrollment of 200 participants experiencing symptoms of anxious misery and 50 healthy comparators ( $n = 250$ ). Participants were recruited using a wide range of methods including flyers, online advertisements, social media and brochures in clinics. Interested participants were prescreened via a phone or online survey and were scheduled for an in-person screening if they met preliminary eligibility criteria. Full inclusion/exclusion criteria for participation in the study (Table 2) were verified during the in-person screening. Exclusionary criteria included MRI contraindications (impairing claustrophobia, aneurysm clips, shunts, non-removable body piercings, non-removable cochlear or ear implants, permanent dentures or dental implants, joint replacements or prosthesis, pacemakers, defibrillators, or other implanted metal devices), histories of certain neurological or cognitive disorders and events (amyotrophic lateral sclerosis, brain aneurysms, brain injury, brain tumors, cerebral palsy, Chiari malformation, dementia, encephalopathy, multiple sclerosis, Parkinson’s disease, recurrent epilepsy or seizures, stroke, or transient ischemic attacks), histories of exclusionary psychiatric conditions (bipolar I, schizophrenia, schizophreniform disorder, schizoaffective disorder, or psychosis) or any other factors that in the investigator’s judgement may have affected patient safety or compliance.

Given that participant recruitment and data collection was local to Philadelphia, USA, this project strived to attain a racially and ethnically diverse sample to reflect the diversity of the city of Philadelphia and the US population at large (LeWinn et al., 2017). This study oversampled female participants to approximate sex disparities in the prevalence of anxious misery disorders (Cyranowski et al., 2000). Sex was defined as biological sex assigned at birth; current gender identity was also

**Table 1**  
Participant characteristics.

%	Category	Total (N = 121)	Control (N = 24)	Anxious Misery (N = 97)
<b>Sex</b>				
71.1%	Female	86	17	69
28.9%	Male	35	7	28
<b>Age (median = 26)</b>				
28.9%	18–23 y/o	35	7	28
35.5%	24–29 y/o	43	9	34
19.0%	30–35 y/o	23	5	18
11.6%	36–41 y/o	14	2	12
2.5%	42–47 y/o	3	1	2
0.0%	48–53 y/o	0	0	0
2.5%	54–59 y/o	3	0	3
<b>Race</b>				
12.4%	Asian	15	3	12
20.7%	Black	25	4	21
5.8%	Multiracial	7	1	6
3.3%	Other	4	1	3
4.9%	Undisclosed	6	0	6
52.9%	White	64	15	49
<b>Ethnicity</b>				
5.0%	Hispanic	6	0	6
92.5%	Not Hispanic	112	24	88
2.5%	Undisclosed	3	0	3
<b>Medication status</b>				
26.8%	Medicated	–	–	26
73.2%	Unmedicated	–	–	71

Education and employment characteristics are detailed in Supplementary Table 1. Descriptions of medication use are detailed in Supplementary Table 2.

**Table 2**  
Summary of inclusion and exclusion criteria.

Inclusion Criteria	Exclusion Criteria
<p><b>Patients</b> exhibited sufficiently high neuroticism score based on the NEO FFI (at least one standard deviation above a point estimate of the general adult population mean*)</p> <p><b>Controls</b> did not meet DSM-5 criteria (currently or historically) for the diagnosis of any psychiatric or cognitive disorder and exhibited sufficiently low neuroticism based on the NEO FFI (at least one standard deviation below a point estimate of the general adult population mean*)</p> <p>Age 18–60</p> <p>Fluent in English (written and oral)</p>	<p>History of exclusionary neurological or cognitive disorder(s)/event(s), psychiatric conditions, or mood disorders, including schizophrenia and bipolar I</p> <p>Current substance use disorder (as defined by the DSM-5), including addiction to alcohol, recreational drugs (e.g. cocaine, heroin, and methamphetamines), or prescription medication</p> <p>MRI contraindication</p> <p>HIV positive</p> <p>Active Hepatitis B or Hepatitis C</p> <p>Female participant was pregnant, breastfeeding, or trying to become pregnant</p>

\* Mean NEO-FFI neuroticism scores were determined from separate distributions for males (mean = 19.1, sd = 7.1) and females (mean = 22.2, sd = 7.9) based on previously collected data from a sample of 635 adults (McCrae et al., 2007).

collected.

We did not require participants to cease taking psychotropic medication that they were currently taking, although current addiction to alcohol, recreational drugs or prescription medications was exclusionary. The majority of our study participants (73.2%) were unmedicated, and extensive efforts were made to record any past or present medication use (see Supplementary Table 2 for a summary of medication use).

## 2.2. Study groupings and clinical classification

For group-level analyses, participants were placed into either the healthy control (HC) or anxious misery (AM) groups. Group assignment was based on participants' raw Neuroticism score on the Neuroticism-Extraversion-Openness Five-Factor Inventory (NEO FFI; (McCrae et al., 2007) collected during Visit 1. Neuroticism was selected as an eligibility criterion because it captures general elements of psychopathology that are shared by participants diagnosed with depression, anxiety and trauma-related disorders (Andrews et al., 1990; Khan et al., 2005). Importantly, it also does not overlap with the diagnostic criteria of any Axis I disorders in the DSM-5, helping to ensure a truly transdiagnostic dataset. Based on previously collected data from a sample of 635 adults (McCrae et al., 2007), AM participants were required to have raw Neuroticism scores at least 1 standard deviation above the mean, which had different distributions for males (raw score  $\geq 26.2$ ) and females (raw score  $\geq 30.1$ ). There were seven AM participants recruited in the first month of the project, prior to the implementation of the NEO threshold, whose NEO scores were above the mean but not by a full standard deviation. HC participants were required to have raw Neuroticism scores at least one standard deviation below the mean (by sex) and were excluded if they met the criteria for a current diagnosis of any psychiatric disorder.

Diagnoses of current psychiatric disorders according to the DSM-5 were provided using the Structured Clinical Interview for DSM-5 (SCID-5). Diagnoses were provided either directly by a psychiatrist or a SCID-certified clinical research coordinator under the supervision of a psychiatrist. Aside from these exclusionary diagnoses, depressive, anxious or trauma-related SCID diagnoses were not used to determine eligibility; rather, they were obtained for comparison purposes in future analyses.

## 2.3. Participant schedule

A schematic of the study schedule is presented in Fig. 1. Interested participants who completed the phone or online screening survey were eligible for an in-person screening (Visit 1). During Visit 1, participants provided informed consent before any study-related procedures were conducted. Screening procedures included an evaluation of medical history (e.g., hospitalizations, psychiatric medication use), a structured diagnostic interview (SCID-5) to determine current anxious misery diagnoses and a collection of demographic information. If the individual was confirmed to be eligible for the study, they also completed a series of clinician-administered measures, the Penn Computerized Neurocognitive Battery (Penn CNB) for neurocognitive assessment and several self-report assessments of thoughts, mood and behaviors. Completion of Visit 1 took approximately 3–4 h.

At the beginning of Visit 2, participants were taken to a Siemens Prisma 3 T scanner for an MRI scan. After the MRI scan, participants completed the NIH Toolbox Neurocognitive and Emotion batteries (see Supplementary Tables 5, 7). Completion of Visit 2 took approximately 3–4 h. Attempts were made to minimize the time between Visits 1 and 2. 82.6% of participants were imaged within two weeks of Visit 1, and 94.2% were imaged within three weeks.

## 3. Protocol: Self-report and clinician-administered measures

### 3.1. Clinically relevant dimensional measures

A rich array of clinical measures were selected to operationalize cognition and behavior beyond traditional diagnostic categorizations. Eligible participants completed a total of 32 self-report measures as well as clinician-administered measures, including measures of behavior, thoughts, health, mood, life stress and trauma (Table 3, Supplementary Tables 3 and 4 for detailed descriptions of each instrument). 14 of these measures came from the National Institutes of Health (NIH) Emotional Batteries, a set of computerized measures that overlap with those administered in other HCP studies (Gershon et al., 2013; Mungas et al., 2014).

### 3.2. Cognitive and neuropsychological measures

Cognitive and neuropsychological function measures were selected from the National Institutes of Health (NIH) Toolbox (Gershon et al., 2013; Mungas et al., 2014) and the University of Pennsylvania Computerized Neurocognitive Battery (Penn CNB; (Gur, 2001; Gur et al., 2010; Moore et al., 2015). Please refer to Table 4 for a list of each task and Supplementary Tables 5–6 for detailed descriptions of each task. Participants completed a total of 12 computerized measures from these standardized batteries, 6 of which are from the NIH Toolbox Cognition Batteries. We selected measures to assess a range of cognitive domains and provide deep cognitive phenotyping for those domains expected to

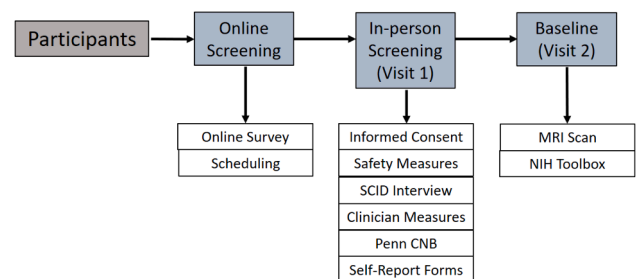


**Fig. 1.** Schematic of the participant schedule for both healthy controls and clinical participants. Listed below each event of the study are the procedures that participants completed for that event. The majority of participants (82.6%) completed Visit 2 within two weeks of Visit 1.

**Table 3**  
Clinically relevant dimensional measures (self-report and clinician-administered).

Domain	Measure	Subscale
Hedonic capacity	Snaith-Hamilton Pleasure Scale (SHAPS; Snaith et al., 1995)	
Anxious and depressive symptoms	Anxiety Depression Distress Inventory-27 (ADDI-27 / MASQ-Short; Taylor et al.,)	Positive Affect Somatic Anxiety General Distress
Anxiety sensitivity	Anxiety Sensitivity Index-3 (ASI-3; Reiss et al., 1986)	Physical Concerns Cognitive Concerns Social Concerns
State and quasi-trait anxiety	Anxiety 8 – PROMIS (Pilkonis, 2011)	
Insomnia	Insomnia Severity Index (ISI; Bastien et al., 2001)	
Motivational systems	Behavioral Inhibition and Activation questionnaire (BIS-BAS Carver and White,)	BIS BAS-Drive BAS-Fun BAS-Reward
Rumination	Ruminative Thought Style Questionnaire (RTSQ; Nolen-Hoeksema et al.,)	
Life stress and trauma	Childhood Trauma Questionnaire (CTQ; Bernstein, 1994)	Emotional Abuse Physical Abuse Sexual Abuse Emotional Neglect Physical Neglect
	Holmes-Rahe Life Stress Inventory Noone, 20172017)	
	Maltreatment and Abuse Chronology of Exposure (MACE; Bernstein, 1994)	
	PTSD Checklist for DSM-5 (PCL-5; (Blanchard et al., 1996)	Severity
	Life Events Checklist for DSM-5 (LEC-5; Michalos and Kahlke, 2014)	Multiplicity
General health	12-item Short-Form Health Survey (SF-12; WARE et al., 1996)	
	Sheehan Disability Scale (SDS; (Sheehan et al., 1996)	
Acute pain	Visual Analog Scale for Pain (VAS; Kertzman et al., 2004)	
Nicotine dependence	Fagerstrom Test for Nicotine Dependence (FTND; Heatherton et al., 1991)	
Social adjustment	Social Adjustment Scale - Self Report (SAS-SR; Weissman and Bothwell, 1976)	
Threat sensitivity	20-item Trait Fear inventory (TF-20; Marks and Mathews, 1979)	
Depressive symptoms	Montgomery-Asberg Depression Rating Scale (MADRS; Montgomery and Asberg, 1979)	
	Hamilton Depression Rating Scale (HAM-D / HDRS; Hamilton, 1960)	
Suicide	Columbia-Suicide Severity Rating Scale (C-SSRS; Posner and Columbia-, , 2016)	Past 3 Months
Negative affect*	Anger	Lifetime Affect Hostility Physical Aggression Affect
	Fear	Somatic
	Sadness	
Psychological well-being*	Positive Affect General Life Satisfaction Meaning and Purpose	
Social cognition*	Emotional Support Instrumental Support Loneliness FriendshipPerceived Hostility Perceived Rejection Stress and Self-Efficacy Self-Efficacy	

\* All instruments in these domains are from the National Institutes of Health Toolbox Emotional Batteries.

**Table 4**  
Cognitive and Neuropsychological Measures.

Domain	Tasks	Battery
Cognitive control/attention	Flanker Inhibitory Control and Attention Test	NIH Toolbox
Cognitive flexibility	Dimensional Change Card Sort	NIH Toolbox
Complex cognition	Penn Matrix Analysis Test	Penn CNB
Episodic memory	Picture Sequence Memory Test Penn Word Memory Test Penn Word Memory Test - Delayed Recall	NIH Toolbox Penn CNB Penn CNB
Impulsivity/self-regulation	Delayed Discounting	Penn CNB
Processing speed	Pattern Comparison Processing Speed Test Penn Trailmaking Test, Part A	NIH Toolbox Penn CNB
Social cognition	Emotion Recognition Test	Penn CNB
Vocabulary knowledge	Picture Vocabulary Test	NIH Toolbox
Working memory	List Sorting Working Memory Test	NIH Toolbox

NIH Toolbox = National Institutes of Health Toolbox Cognition Batteries; Penn CNB = University of Pennsylvania Computerized Neurocognitive Battery.

be most associated with NVS dysfunction (e.g. attention, working memory, executive control, episodic memory, processing speed) based on prior work (Etkin et al., 2013; Scott et al., ; Snyder,).

#### 4. Protocol: Imaging

##### 4.1. Procedures and hardware

Participants were scanned using a Siemens Prisma 3 T whole-body MRI system equipped with a 64-channel head/neck array with 80mT/m maximum gradient amplitude and a 200 T/m/s maximum slew rate. Stimuli were presented using an MRI-compatible LCD panel (InVivo SensaVue), with responses collected via a 4-button response box corresponding to the four non-thumb digits, held in the right hand. All participants had a heart rate monitor attached to their left index finger during scanning and a respiration belt placed around their diaphragm. In order to ensure consistency across participant sessions, all technicians followed a uniform procedure during scanning.

##### 4.2. Data management

Imaging data was stored and managed using the Flywheel infrastructure (<https://flywheel.io/>); preprocessing took place on the Penn Center for Biomedical Image Computing and Analytics (CBICA) high performance computing cluster, a secure computing cluster housed at the University of Pennsylvania. Only personnel with study approval were able to access these data. All protected health information was stored on REDCap, a secure web application for managing clinical research databases ([www.project-redcap.org](http://www.project-redcap.org)).

##### 4.3. Imaging protocols

Please refer to Table 5 for an overview of the scanning sequence. All scans were calibrated automatically via onboard Siemens autoalign software, followed by a visual inspection from the operator to ensure that the FOV and alignment are correct.

**Table 5**  
Acquisition Sequence.

	Modality	PE	Volumes	Duration (min.)	Resolution (mm)	Stimulus
1	Localizer	-	-	0:09	1.2 × 1.2 × 5.0	-
2	AAHeadScout	-	-	0:17	1.6 × 1.6 × 1.6	-
3	Localizer (aligned)	-	-	0:21	1.2 × 1.2 × 5.0	-
4	Bias Correction Map	-	-	0:26	2.0 × 2.0 × 2.0	-
5	Bias Correction Map (64CH)	-	-	0:26	2.0 × 2.0 × 2.0	-
6	Spin Echo	AP	3	0:32	2.0 × 2.0 × 2.0	-
7		PA	3	0:32	2.0 × 2.0 × 2.0	-
8	Resting-state fMRI	AP	420	5:46	2.0 × 2.0 × 2.0	Fixation
9		PA	420	5:46	2.0 × 2.0 × 2.0	Fixation
10	T1w	-	1	6:38	0.8 × 0.8 × 0.8	-
11	T2w	-	1	5:57	0.8 × 0.8 × 0.8	-
12	Spin Echo	AP	3	0:32	2.0 × 2.0 × 2.0	-
13	Spin Echo	PA	3	0:32	2.0 × 2.0 × 2.0	-
14	Resting-state fMRI	AP	420	5:46	2.0 × 2.0 × 2.0	Fixation
15		PA	420	5:46	2.0 × 2.0 × 2.0	Fixation
16	T2w - Hippocampus	-	1	8:10	0.4 × 0.4 × 1.2	-
17	Conflict fMRI	AP	290	4:02	2.0 × 2.0 × 2.0	Conflict
18		PA	290	4:02	2.0 × 2.0 × 2.0	Conflict
19		AP	290	4:02	2.0 × 2.0 × 2.0	Conflict
20		PA	290	4:02	2.0 × 2.0 × 2.0	Conflict
21	dMRI	AP	1	5:37	1.5 × 1.5 × 1.5	-
22		PA	1	5:37	1.5 × 1.5 × 1.5	-
23		AP	1	5:41	1.5 × 1.5 × 1.5	-
24		PA	1	5:41	1.5 × 1.5 × 1.5	-
25	Faces fMRI	AP	340	4:42	2.0 × 2.0 × 2.0	Faces
26		PA	340	4:42	2.0 × 2.0 × 2.0	Faces
27	Gambling fMRI	AP	228	3:12	2.0 × 2.0 × 2.0	Gambling
28		PA	228	3:12	2.0 × 2.0 × 2.0	Gambling

Note. PE = phase encoding; AP = anterior to posterior phase encoding; PA = posterior to anterior phase encoding.

#### 4.4. Structural imaging

##### 4.4.1. Acquisition parameters

1. T1-weighted: TE = 2.22 ms, TR = 2.40 s, FA = 8, acquisition time = 6:38, FOV = 256 × 256 mm, slice thickness = 0.80 mm, fat suppression = water excitation, orientation = sagittal, receiver bandwidth = 220 Hz/Px.

2. T2-weighted: TE = 563.00 ms, TR = 3.20 s, acquisition time = 5:57, FOV = 256 × 256 mm, slice thickness = 0.80 mm, fat suppression = none, orientation = sagittal, receiver bandwidth = 744 Hz/Px.
3. Spin Echo: TE = 66.00 ms, TR = 8.00 s, FA = 90, acquisition time = 0:32, FOV = 208 mm × 208 mm, slice thickness = 2.00 mm, slice orientation = T > C-20.0, phase encoding = AP and PA, echo spacing = 0.58 ms, fat suppression = fat saturation, receiver bandwidth = 2290 Hz/Px.
4. Single-band calibration: TE = 1.03 ms, TR = 0.25 s, FA = 3, acquisition time = 0:26, FOV = 256 mm × 256 mm, slice thickness = 2.00 mm, slice orientation = sagittal, phase encoding = AP and PA, echo spacing = 3.1 ms, fat suppression = none, receiver bandwidth = 540 Hz/Px.
5. T2-weighted hippocampus: TE = 80.0 ms, TR = 9.24 s, FA = 180, acquisition time = 8:10, FOV = 180 × 180 mm, slice thickness = 1.20 mm, fat suppression = none, orientation = C > T-26.8, receiver bandwidth = 100 Hz/Px.

##### 4.4.2. Hippocampus imaging

We collected a dedicated T2-weighted MRI of the hippocampus, to be analyzed using an automated subfield segmentation technique (Yushkevich et al., 2010). The appearance of the hippocampus in standard T1-weighted scans is largely indistinguishable between subjects, necessitating more precise imaging methods. This acquisition-analysis pipeline has been shown to be comparable to manual segmentation methods, while being more efficient and less susceptible to inter-rater bias (Yushkevich et al., 2010).

#### 4.5. Diffusion imaging

Diffusion imaging was conducted while participants viewed a blank screen. Participants were allowed to close their eyes but were instructed to remain awake. Two pairs of acquisitions with opposite phase encoding were collected. Further, to improve registration to the structural image, an anatomical coplanar image was also collected.

##### 4.5.1. Acquisition parameters

1. Diffusion-weighted: 2 pairs of acquisitions = 4 acquisitions total, TE = 89.20 ms, TR = 3.23 s, acquisition time = 5:37, FOV = 210 mm × 210 mm, slice orientation = T > C-20.0, FA = 78, phase encoding = AP and PA, echo spacing = 0.69 ms, voxel size = 1.5 mm isotropic, diffusion weightings = 2, b-Values = 1500, 3000 s/mm<sup>2</sup>, # of directions = 93 (b = 1500), 92 (b = 3000), # of b0 = 14.

#### 4.6. Functional imaging

All functional scans were acquired using multi-band EPI sequences with identical parameters. To correct for susceptibility distortions, two pairs of spin echo fieldmaps with opposite phase encoding directions (one anterior-posterior, the other posterior-anterior) were acquired during the scanning session. Similarly, each task was conducted in pairs of scans with opposite phase encoding directions (some scans, like resting state and the emotional interference task, had two pairs of scans). To improve registration to the structural scan, an anatomical coplanar image was also acquired.

##### 4.6.1. Acquisition parameters

1. EPI fMRI: TE = 37.00 ms, TR = 0.80 s, FA = 52, multi-band acceleration factor = 8, resting-state acquisition time = 5:46, EIT acquisition time = 4:02, IPT acquisition time = 3:12, EPT acquisition time = 4:42, FOV = 208 × 208 mm, slice orientation = T > C-20.0, phase encoding = AP/PA, echo spacing = 0.58 ms, number of volumes = 420, slice thickness = 2.00 mm, fat suppression = fat saturation, receiver bandwidth = 2290 Hz/Px.

2. Spin Echo: TE = 66.00 ms, TR = 8.00 s, FA = 90, acquisition time = 0.32, FOV = 208 mm × 208 mm, slice thickness = 2.00 mm, slice orientation = T > C-20.0, phase encoding = AP and PA, echo spacing = 0.58 ms, fat suppression = fat saturation, receiver bandwidth = 2290 Hz/Px.

#### 4.6.2. Functional imaging tasks

**Emotional interference task (EIT):** This task aims to capture deficits in cognitive control in the presence of negatively valenced emotional distractors. In this event-related design adapted from [Fales et al. \(2008\)](#) and [Vuilleumier et al. \(2001\)](#), participants are instructed to indicate through button press whether two pictures on either the horizontal or vertical axes are identical or different ([Fig. 2a](#)). After a cue indicating which axis to attend to, four images are briefly shown on the top, bottom, left and right of the screen, and participants are given a short period to respond.

Images are either human faces or houses. Further, faces can have either a neutral expression or a fearful one. Images sharing an axis will always be of the same category and emotion, if applicable. Therefore, there are four conditions of interest that were entered into our task modeling procedures: attending to fearful faces, attending to neutral faces, ignoring fearful faces and ignoring neutral faces. Each condition is presented 24 times across all runs of this task.

After a 1 s fixation cross, images are presented for 250 ms, and participants are allotted 2.2 s to respond. Intertrial intervals of 2150, 4660, 9680 and 12190 ms are randomly and equally distributed throughout each run. Total run duration is 3:54 and the task is run 4 times, resulting in a total scan time of 15:36 for this task.

**Emotional processing task (EPT):** This task aims to capture abnormalities in the processing of emotional faces and follows the same design as the one implemented in the HCP ([Van Essen et al., 2013](#)). In this block-related design originally adapted from [Hariri et al. \(2002\)](#); participants are presented with three images and are instructed to indicate through button press whether the image on the left or the image on the

right matches the image at the top ([Fig. 3a](#)). Images can belong to one of four categories: fearful faces, neutral faces, happy faces and control stimuli (e.g. fruits and vegetables). These four categories were the four event types entered into our task modeling procedures.

Images are present for 3 s each and each block is composed of six images of the same category, resulting in a block duration of 18 s. Each of the four categories, in addition to a baseline condition (white fixation cross on a black background), is allocated three blocks, resulting in a total run time of 4:32. Each participant completes two runs, resulting in a total scan time of 9:04 for this task.

**Incentive processing task (IPT):** This task addresses neural abnormalities in reward processing and follows the same design as the one implemented in the HCP ([Van Essen et al., 2013](#)). In this block-related design originally adapted from [Delgado et al. \(2000\)](#), a question mark is presented on screen, and participants have to guess whether the number obscured by the question mark (which can range 1–9) is greater than or less than five ([Fig. 4a](#)). If the participant guesses correctly, a green arrow pointing upwards with text indicating “+\$1.00” is shown. If the participant guesses incorrectly, the participant sees a red arrow pointing downwards with text indicating “-\$0.50”. If the number was five, a gray double-headed arrow is presented, indicating that money was neither gained nor lost. If the participant does not respond within the time allocated for the trial (1.5 s after the question mark is presented), then the text “no response” is presented, along with an indication that no money is gained or lost that round. Participants were told that they should perform the task as if they would earn real money, but no rounds were actualized in participant payoff.

Unknown to the participant, the sequence of “reward” and “loss” trials is pre-set such that blocks of stimuli are composed of primarily reward and primarily loss trials. To obscure this, a primarily “reward” block will always contain two “neutral” or “loss” trials and vice-versa for primarily “loss” blocks. Trial types are pseudo-randomized within each block. Tasks were modeled using an event-wise design with three event types: “reward”, “neutral” and “loss”. Timings corresponded to the onset

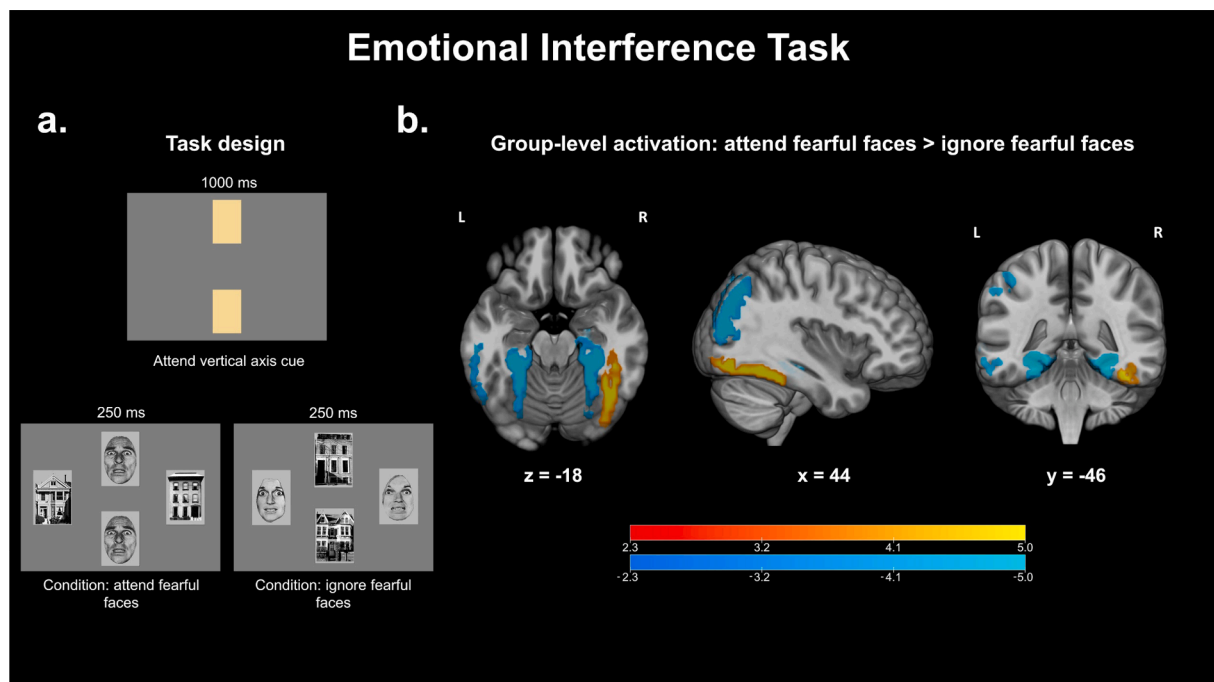


**Fig. 2.** *a.* Task design for the Emotional Interference Task. After a 1000 ms cue indicating which set of stimuli to attend to (above), two faces and two houses are flashed on the screen for 250 ms (below). Participants are allotted 2200 ms to respond whether the attended stimuli were the same or different. *b.* Z-statistic maps thresholded using Gaussian random field theory (cluster-defining threshold,  $z > 2.3$ ; cluster extent threshold,  $p < 0.01$ ). Warm colors indicate significant clusters for the attend fearful faces > ignore fearful faces contrast while cool colors indicate significant clusters for the ignore fearful faces > attend fearful faces contrast. Coordinates of slices are in MNI space. Color bars indicate Z-statistics.

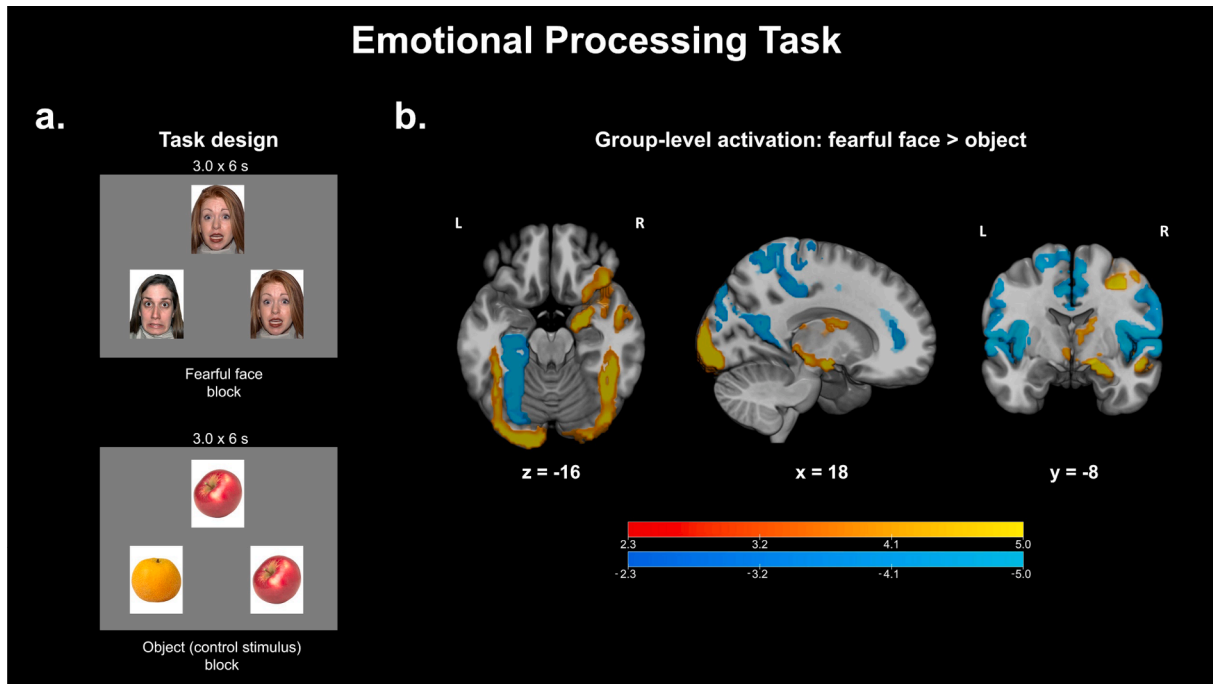


**Fig. 3.** *a.* Task design for the Emotional Processing Task. Participants view three images at a time for 3 s and are instructed to indicate whether the picture on the left or right matches the picture in the center. Each block is composed of 6 sets of images. *b.* Z-statistic maps thresholded using Gaussian random field theory (cluster-defining threshold,  $z > 2.3$ ; cluster extent threshold,  $p < 0.01$ ). Warm colors indicate significant clusters for the fearful face > object contrast while cool colors indicate significant clusters for the object > fearful face contrast. Coordinates of slices are in MNI space. Color bars indicate Z-statistics.

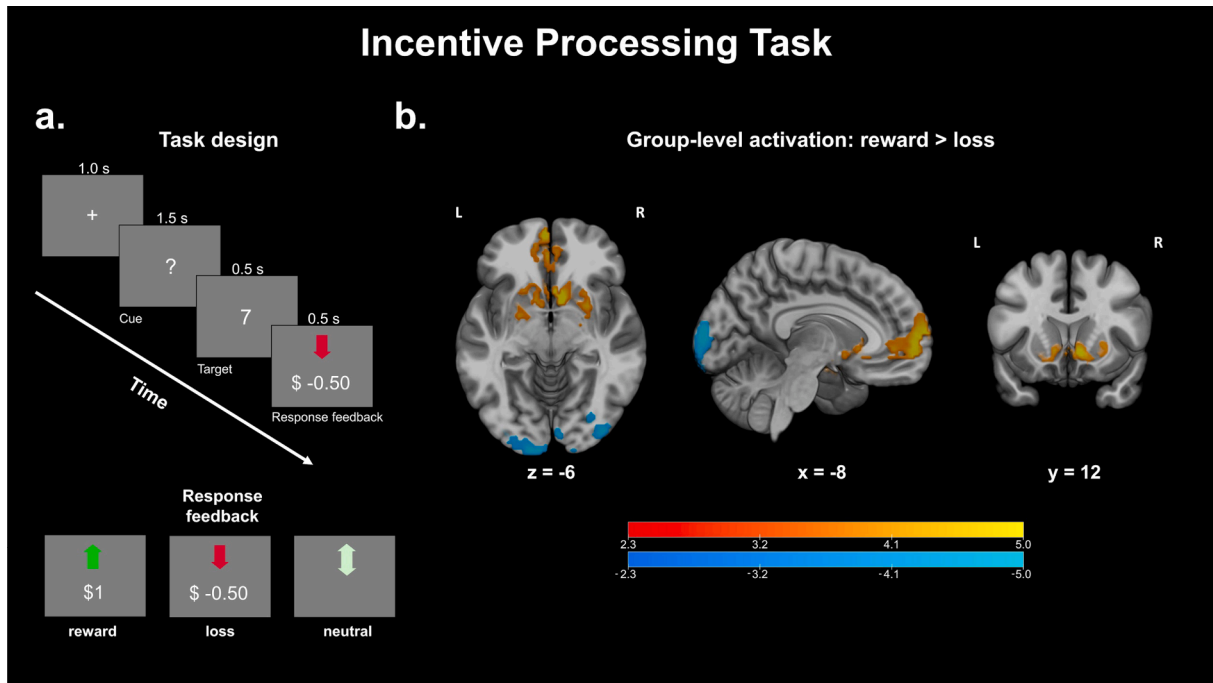


**Fig. 4.** *a.* Task design for the Incentive Processing Task. During a 1.5 s cue, participants guess whether a hidden number is greater than or less than five, after which feedback images are shown for 1 s. The timeline of events is illustrated above, while the three possible response feedback stimuli are illustrated below. *b.* Z-statistic maps thresholded using Gaussian random field theory (cluster-defining threshold,  $z > 2.3$ ; cluster extent threshold,  $p < 0.01$ ). Warm colors indicate significant clusters for the reward > loss contrast while cool colors indicate significant clusters for the loss > reward contrast. Coordinates of slices are in MNI space. Color bars indicate Z-statistics.

of the response feedback portion of the task.

Each trial is composed of the question mark cue for 1.5 s, followed by feedback images for 1.0 s. Each trial is separated by a 1.0 s inter-trial interval. Blocks are composed of 8 trials each, resulting in a block

length of 28 s. Runs are composed of two “reward” blocks, two “loss” blocks and a baseline condition block (fixation cross, 15 s), for a total run duration of 3:02. Each participant completes two runs, for a total scan time of 6:04 for this task.

#### 4.6.3. Resting-state fMRI

During resting state scans, participants viewed a gray screen with a white crosshair (Fig. 5a). Participants were instructed to fixate on the crosshair, while blinking normally and keeping their eyes open. This was performed in two sets of two, for a total of four scans, each of which lasted for 5:46 min (resulting in a total scan time of 23:04 for resting state). Participants were given a series of follow-up questions after each run concerning their mental state during the scan (e.g. frequency of thought wandering, frequency of sleeping) and responded via the 4-button box.

#### 4.7. Image preprocessing and analysis

##### 4.7.1. Structural and functional imaging

All structural and functional images were processed using FMRI-PREP, a well-validated preprocessing pipeline. Note that data will also be preprocessed using the HCP minimal preprocessing pipelines (Glasser et al., 2013) upon public release of this dataset to the NDA. The following is boilerplate text provided by FMRI-PREP describing the steps taken during preprocessing.

Results included in this manuscript come from preprocessing performed using FMRI-PREP version stable (Esteban et al., 2019), a Nipype (Gorgolewski, 2011) based tool. Each T1w (T1-weighted) volume was corrected for INU (intensity non-uniformity) using N4BiasFieldCorrection v2.1.0 (Tustison et al., 2010) and skull-stripped using ants-BrainExtraction.sh v2.1.0 (using the OASIS template). Spatial normalization to the ICBM 152 Nonlinear Asymmetrical template version 2009c (Fonov et al., 2009) was performed through nonlinear registration with the antsRegistration tool of ANTs v2.1.0 (AVANTS et al., 2008), using brain-extracted versions of both T1w volume and template. Brain tissue segmentation of cerebrospinal fluid (CSF), white-matter (WM) and gray-matter (GM) was performed on the brain-extracted T1w using fast (Zhang et al., 2001) (FSL v5.0.9).

Functional data was motion corrected using mcflirt, calculating one rigid-body transform for each BOLD time-step (FSL v5.0.9 (Jenkinson et al., 2002)). Distortion correction was performed using an implementation of the TOPUP technique (Andersson et al., 2003) using

3dQwarp (AFNI v16.2.07 (Cox, 1996)). This was followed by coregistration to the corresponding T1w using boundary-based registration (Greve and Fischl, 2009) with six degrees of freedom, using flirt (FSL). Motion correcting transformations, field distortion correcting warp, BOLD-to-T1w transformation and T1w-to-template (MNI) warp were concatenated and applied in a single step using antsApplyTransforms (ANTs v2.1.0) using Lanczos interpolation.

Physiological noise regressors were extracted applying CompCor (Behzadi et al., 2007). Principal components were estimated for the two CompCor variants: temporal (tCompCor) and anatomical (aCompCor). A mask to exclude signal with cortical origin was obtained by eroding the brain mask, ensuring it only contained subcortical structures. Six tCompCor components were then calculated including only the top 5% variable voxels within that subcortical mask. For aCompCor, six components were calculated within the intersection of the subcortical mask and the union of CSF and WM masks calculated in T1w space, after their projection to the native space of each functional run. Frame-wise displacement (Power et al., 2014) was calculated for each functional run using the implementation of Nipype.

Many internal operations of FMRI-PREP use Nilearn (Abraham, 2014), principally within the BOLD-processing workflow. For more details of the pipeline see <https://fmriprep.readthedocs.io/en/stable/workflows.html>.

Resting state data were further preprocessed using the eXtensible Connectivity Pipeline (XCP Engine; (Ciric et al., 2018)). The workflow is summarized as follows: (i) removal of the 10 initial volumes (8 s) to achieve signal stabilization, (ii) demeaning and removal of quadratic trends using a general linear model to account for scanner drift, (iii) intensity despiking using 3dDespike from AFNI (Cox, 1996), (iv) band-pass temporal filtering of time series between 0.01 Hz and 0.08 Hz using a first-order Butterworth filter (Biswal et al., 2010), (v) regression of nine confounding signals (six motion parameters + global signal + mean white matter signal + mean cerebral spinal fluid signal) and as well as the temporal derivative, quadratic term and temporal derivatives of each quadratic term (resulting in 36 regressors total; (Satterthwaite et al., 2013) and (vi) spatial smoothing with SUSAN from FSL (Smith and Brady, 1997) using a 6 mm FWHM kernel.

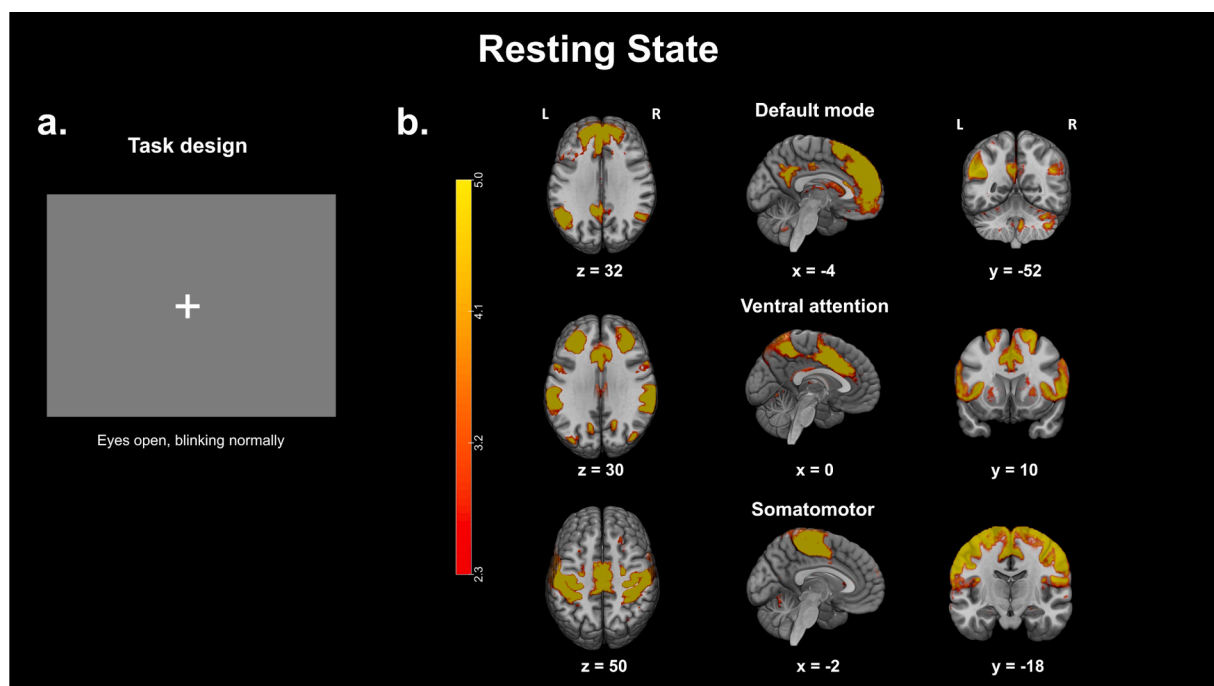


**Fig. 5.** a. Task design for resting state acquisitions. Participants were instructed to lie still with their eyes open, blinking normally. b. Z-statistic spatial weights for three independent components from ICA. For display purposes, weights were thresholded at  $z = 2.3$ . Coordinates of slices are in MNI space.

Task activation maps were generated using FSL (Smith et al., 2004), using a generalized linear modeling (GLM) approach. Task timings were convolved with a double-gamma hemodynamic response function. Variance due to motion was accounted for by including the six translational and rotational motion parameters, plus the temporal derivative, quadratic term and temporal derivatives of each quadratic term (resulting in 24 nuisance regressors total) in the regression model. Parameter estimates from contrasts of interest were combined within-subject using fixed effects modeling and then combined across subjects using hierarchical mixed modeling (using FSL's FLAME). Finally, cluster-based inference using Gaussian random field theory was conducted on the resulting z-statistic image (cluster-defining threshold,  $z > 2.3$ ; cluster extent threshold,  $p < 0.01$ ; easythresh utility in FSL). For the purpose of this descriptive analysis, group-level activation maps for contrasts of interest pooled AM and HC participants together.

We used MELODIC (Multivariate Exploratory Linear Decomposition into Independent Components) version 3.15, part of FSL, to extract functional connectivity networks from preprocessed resting state functional data. Spatial activation patterns were projected onto a 10-dimensional subspace using temporally-concatenated group independent component analysis (ICA) with MELODIC's Incremental Group-PCA (MIGP; (Smith et al., 2014)). MIGP uses an incremental approach to decompose 4D functional data into non-Gaussian spatial source distributions for the estimation of group-average spatial eigenvectors. The 10 strongest spatial eigenvectors underwent an unmixing algorithm to identify spatially-independent group-average network components.

#### 4.7.2. Diffusion imaging

Diffusion weighted images were preprocessed using QSIprep, an open-source software package that configures pipelines for processing diffusion-weighted data (retrieved from <https://github.com/PennBBL/qsiprep>); QSIprep is not affiliated or endorsed by the creators of FMRIPREP). QSIprep includes options to replicate the outputs of the HCP dMRI pipelines (Sotiropoulos et al., 2013). In short, this pipeline performs (i) anatomical preprocessing and spatial normalization to MNI template space using ANTs (Avants et al., 2011), (ii) head motion correction, susceptibility distortion correction and eddy current correction using TOPUP and eddy (Andersson et al., 2003; Smith et al., 2004) and (iii) calculation of generalized fractional anisotropy (GFA) using generalized q-sampling imaging (Yeh et al.,). GFA was sampled along 16 standard tracts from the HCP Diffusion MRI Template (Yeh et al., 2018).

#### 4.7.3. Myelin maps and cortical thickness

In order to generate group average cortical thickness meshes, structural images were preprocessed using the HCP minimal preprocessing pipelines (Glasser et al., 2013), version 4.1.3 (retrieved from <https://github.com/BIDS-Apps/HCPpipelines/releases/tag/v4.1.3>). The *PreFreeSurfer*, *FreeSurfer* and *PostFreeSurfer* workflows were used to process T1w and T2w images. In brief, these workflows performed (i) gradient nonlinearity distortion correction, (ii) coregistration of T1w and T2w images, (iii) bias field correction using spin-echo field maps, (iv) spatial normalization to the MNI template, (v) segmentation of cortical and subcortical structures, (vi) reconstruction onto pial and white matter surfaces and (vii) registration to *32k\_fs\_LR* mesh (Van Essen et al., 2012), a standard space template. For the purpose of this descriptive analysis, the group-average cortical thickness surface pooled AM and HC participants together.

#### 4.7.4. Image quality metrics

Automated image quality assessments were performed on each set of data. The primary metric used to assess image quality for our structural images (T1w, T2w) was signal-to-noise ratio (SNR), which was calculated by dividing the mean white and grey matter intensity by the standard deviation of image intensities in a background ROI containing no tissue. For functional images, we used temporal signal-to-noise ratio

(tSNR), reported as the average tSNR for all brain voxels, including white and grey matter. Finally, diffusion images were assessed using neighbor DWI correlation, a model-free method of assessing diffusion weighted signal quality (Yeh, 2019). Neighbor DWI correlation computes pairwise spatial correlation between each dMRI volume and its "neighbor", meaning another volume that samples the closest point in q-space. The correlations are then averaged over all voxels and pairs of DWI volumes. Generally, a higher quality acquisition should have a higher neighbor correlation.

#### 4.7.5. Comparisons with HCP-YA

As a comparison of image quality and preliminary results, we drew from a representative sample of the HCP Young Adult (HCP-YA) dataset (Van Essen et al., 2013). Given our interests in identifying the neural substrates of the NVS in its pathological state (to be conducted in analyses that are outside of the scope of this report), we prioritized the selection of the healthiest participants in order to minimize any potential symptom overlap with our clinical population. As it is this subset of the HCP-YA with which our data will be harmonized, we present image quality metrics from these data. In order to be considered, participants had to meet the following criteria: (i) No parental history of mental illness; (ii) Adult Self Report scores (adjusted by age and sex) below 65 in the following categories: anxious/depressed, withdrawn, somatic complaints, thought problems, attention problems, aggressive behavior, rule breaking behavior, intrusive thoughts, internalizing, externalizing, total problems; (iii) Semi-Structured Assessment for the Genetics of Alcoholism scores  $< 2$  for childhood conduct problems, panic disorder, agoraphobia, any lifetime depressive episodes, and fewer than two depressive symptoms present; (iv) All relevant scans present. This selection criteria left us with 248 out of 1200 HCP-YA participants, from which we randomly selected 97 healthy controls to match our 97 AM participants, matching for age and sex. Due to the differences in age range in our sample (18–59 yoa) and the HCP-HYA sample (22–36 yoa), we were unable to match precisely for age, resulting in similar means with different distributions. In order to account for potential age and sex related effects on image quality, we utilize linear regression to remove these covariates in any of our statistical tests of image quality.

Throughout our quantitative comparisons of image quality, we also report metrics from our sample of healthy controls in order to assess whether the presence of NVS pathology affects measures of image quality, which could potentially complicate the interpretation of any associations between neural and behavioral data (Roalf et al., 2016; Satterthwaite et al., 2012).

## 5. Results

### 5.1. Functional imaging

EIT: Group-level activation patterns (Fig. 2b) indicate significant activation of the R fusiform gyrus for one contrast of interest, attend fearful faces  $>$  ignore fearful faces (Vuilleumier et al., 2001; Kanwisher et al., 1997) (illustrated by warm colors), and significant activation of bilateral parahippocampal gyri and L posterior middle temporal gyrus for the opposite contrast, ignore fearful faces  $>$  attend fearful faces (Epstein and Kanwisher, 1998) (illustrated by cool colors).

EPT: Group-level activation patterns (Fig. 3b) for fearful face  $>$  object indicate significant activation of the R amygdala and bilateral fusiform gyri (Hariri et al., 2002) (illustrated by warm colors), as well as significant activation of the L posterior parahippocampal gyrus and posterior cingulate gyrus for the opposite contrast, object  $>$  fearful face (Davachi, 2006) (illustrated by cool colors).

IPT: Group-level activation patterns (Fig. 4b) of the contrast of interest, reward  $>$  loss, indicate significant activation of subcortical regions implicated in reward processing (illustrated by warm colors), like the bilateral nucleus accumbens and caudate, as well as the ventromedial prefrontal cortex (O'Doherty et al., 2001).

Resting: MELODIC successfully identified several canonical resting state networks, including the default mode (Raichle et al., 2001), ventral attention (Fox et al., 2006) and somatomotor networks (Geyer, 2004) (Fig. 5b).

## 5.2. Comparison with HCP data

We compared our imaging data with 97 healthy control participants from the HCP-YA dataset who passed our eligibility criteria. While efforts were made to match for age and sex, different recruitment criteria between the HCP-YA and the AM projects resulted in different ranges and distributions of ages (HCP-YA mean age  $\pm$  SD = 29.08  $\pm$  3.62, AM mean age  $\pm$  SD = 28.46  $\pm$  7.99; HCP-YA range = (Bastien et al., 2001; Carver and White, 1994; Nolen-Hoeksema et al., 1993; Bernstein, 1994; Noone, 2017; Blanchard et al., 1996; Michalos and Kahlke, 2014; Ware et al., 1996; Sheehan et al., 1996; Kertzman et al., 2004; Heatherton et al., 1991; Weissman and Bothwell, 1976; Marks and Mathews, 1979; Montgomery and Åsberg, 1979; Hamilton, 1960), AM range = (Taylor et al., 2007; Reiss et al., 1986; Pilkonis, 2011; Bastien et al., 2001; Carver and White, 1994; Nolen-Hoeksema et al., 1993; Bernstein, 1994; Noone, 2017; Blanchard et al., 1996; Michalos and Kahlke, 2014; Ware et al., 1996; Sheehan et al., 1996; Kertzman et al., 2004; Heatherton et al., 1991; Weissman and Bothwell, 1976; Marks and Mathews, 1979; Montgomery and Åsberg, 1979; Hamilton, 1960; Posner, 2016; Gur, 2001; Gur et al., 2010; Moore et al., 2015; Etkin et al., 2013; Scott et al., 2015; Snyder, 2013; Yushkevich et al., 2010; Fales et al., 2008; Vuilleumier et al., 2001; Hariri et al., 2002; Delgado et al., 2000; Glasser et al., 2013; Esteban et al., 2019; Gorgolewski, 2011; Tustison et al., 2010; Fonov et al., 2009; Avants et al., 2008; Zhang et al., 2001; Jenkinson et al., 2002; Andersson et al., 2003; Cox, 1996; Greve and Fischl, 2009; Behzadi et al., 2007); HCP-YA  $n$  female = 58/97, AM  $n$  female = 69/97).

### 5.2.1. Structural imaging

**Cortical thickness.** Penn participants had generally higher mean cortical thickness values (3.11 mm, SD = 0.40 mm) compared to HCP-YA participants (2.65 mm, SD = 0.35 mm), although the relative distributions of thickness values across the brain share similar features between the two projects, as illustrated in Fig. 6.

**SNR.** Structural scans obtained from the Penn sample showed generally higher SNR compared to HCP subjects for both T1w (median HCP = 8.78, median Penn = 10.10) and T2w (median HCP = 5.18, median Penn = 8.29). One-way analysis of variance (ANOVA) tests controlling for age and sex revealed significant differences between groups for both T1w and T2w SNR (results summarized in Fig. 7). Post-hoc Tukey tests revealed significantly greater T1w SNR in our anxious misery and healthy participants compared to the HCP-YA (anxious misery & HCP-YA,  $t(97.7) = 5.934, p < .001$ ; healthy comparators & HCP-YA,  $t(27.7) = 17.488, p < .001$ ) and similarly for T2w SNR (anxious misery & HCP-YA,  $t(187.8) = 7.554, p < .001$ ; healthy comparators & HCP-YA,  $t(29.2) = 3.833, p < .001$ ). Our anxious misery and healthy participants did not differ in T1w SNR ( $t(110) = -0.522, p = 0.603$ ) or T2w SNR ( $t(37.3) = -0.700, p = 0.488$ ). No significant age or sex effects were detected.

### 5.2.2. Functional imaging

Following preprocessing, mean root mean squared movement (RMS) was calculated for each scan, across all participants, and scans exceeding a predetermined threshold (RMS > median(RMS) + 3 \* interquartile range) were excluded from further analyses of image quality, as well as analyses of task activation and resting state networks. A “scan” included all volumes of a single acquisition (i.e. a single row of Table 5). If all of a subject’s scans exceed this threshold, they were dropped entirely from the analyses for that task. Two subjects were removed from resting state analyses due to movement; 35 total scans were removed from resting state due to movement. For the EIT, two subjects were cut and 39 scans removed; for the EPT, one subject was cut and seven scans removed; for the IPT, two subjects were cut and six scans removed.

**tSNR.** Across all functional scans, one-way ANOVAs did not detect significant differences between groups, controlling for age and sex. Scans for EIT showed good tSNR across all Penn subjects ( $M = 22.18, SD = 3.11$ ), as did EPT ( $M = 21.93, SD = 2.95$ ), IPT ( $M = 22.52, SD = 2.74$ ) and rfMRI ( $M = 21.89, SD = 2.60$ ). Results are summarized in Fig. 8. No significant age or sex effects were detected.

### 5.2.3. Diffusion imaging

**Neighbor correlation.** Diffusion scans obtained from the Penn sample showed generally higher neighbor correlation compared to HCP subjects (median HCP = 0.63, median Penn = 0.81). A one-way ANOVA controlling for age and sex revealed significant differences between groups (results are summarized in Fig. 9). Post-hoc Tukey tests revealed that both anxious misery individuals and healthy comparators had higher neighbor correlations than HCP-YA participants (anxious misery & HCP-YA,  $t(167.5) = 20.223, p < .001$ ; healthy comparators & HCP-YA,  $t(35.1) = 10.34, p < .001$ ). Our anxious misery and healthy participants did not differ in neighbor correlation ( $t(28.4) = 1.24, p = .222$ ). No significant age or sex effects were detected.

**Trackwise profiles of GFA.** GFA values sampled along 16 standard tracts revealed similar average profiles between the Penn and HCP samples (Fig. 10, shaded area = standard deviation), although participants in the Anxious Misery project had generally higher GFA values.

## 6. Discussion

### 6.1. Comparison to HCP-YA acquisition

Based on the above SNR and structural measures, our data shows comparable quality with HCP-YA data, with higher measures of SNR in T1w/T2w images, equivalent measures of tSNR in functional images and higher neighbor correlation in diffusion-weighted images. Differences in T1w/T2w SNR may partially be explained by the background region-of-interest method that we utilized. Given that multi-element receive coils (like those used in the HCP-YA and Anxious Misery protocols) do not guarantee spatially uniform levels of noise, SNR calculated using “signal-free” regions may not accurately represent a true difference in data quality. However, alternative methods of calculating SNR are problematic for other reasons; for example, calculating contrast-to-noise requires the identification of uniform regions of gray and white matter, but coil shading makes such identifications difficult.

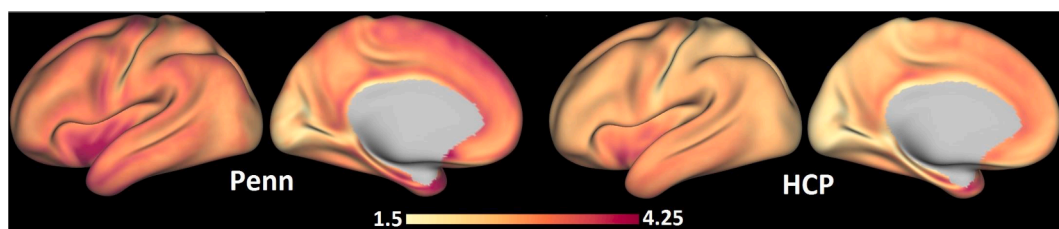


Fig. 6. Comparison of cortical thickness between Penn and HCP samples. Values reported in mm. HCP = Human Connectome Project.

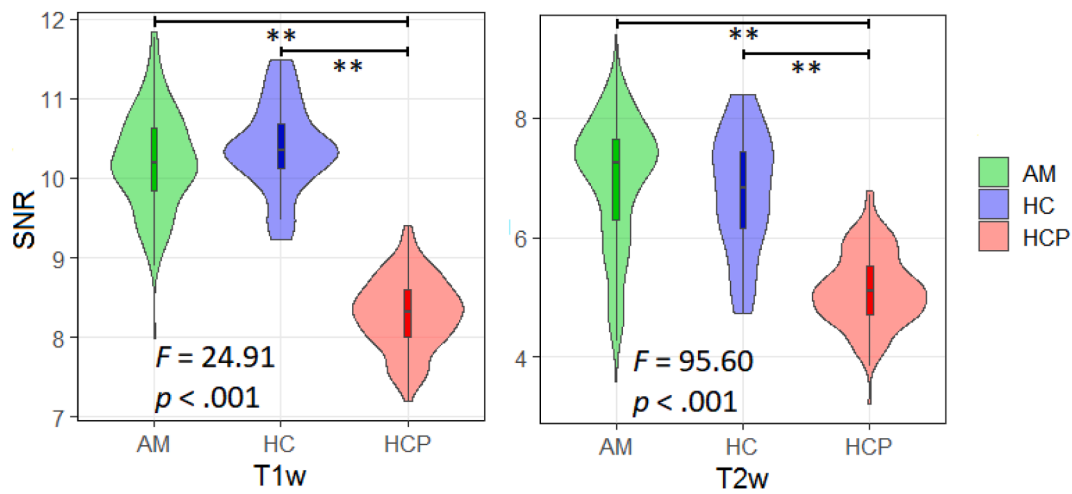


Fig. 7. Signal-to-noise ratio (SNR) for T1w and T2w scans. AM = anxious misery (n = 97), HC = healthy control (n = 24), HCP = Human Connectome Project (n = 97). \*\* = significant at  $p < .001$ .

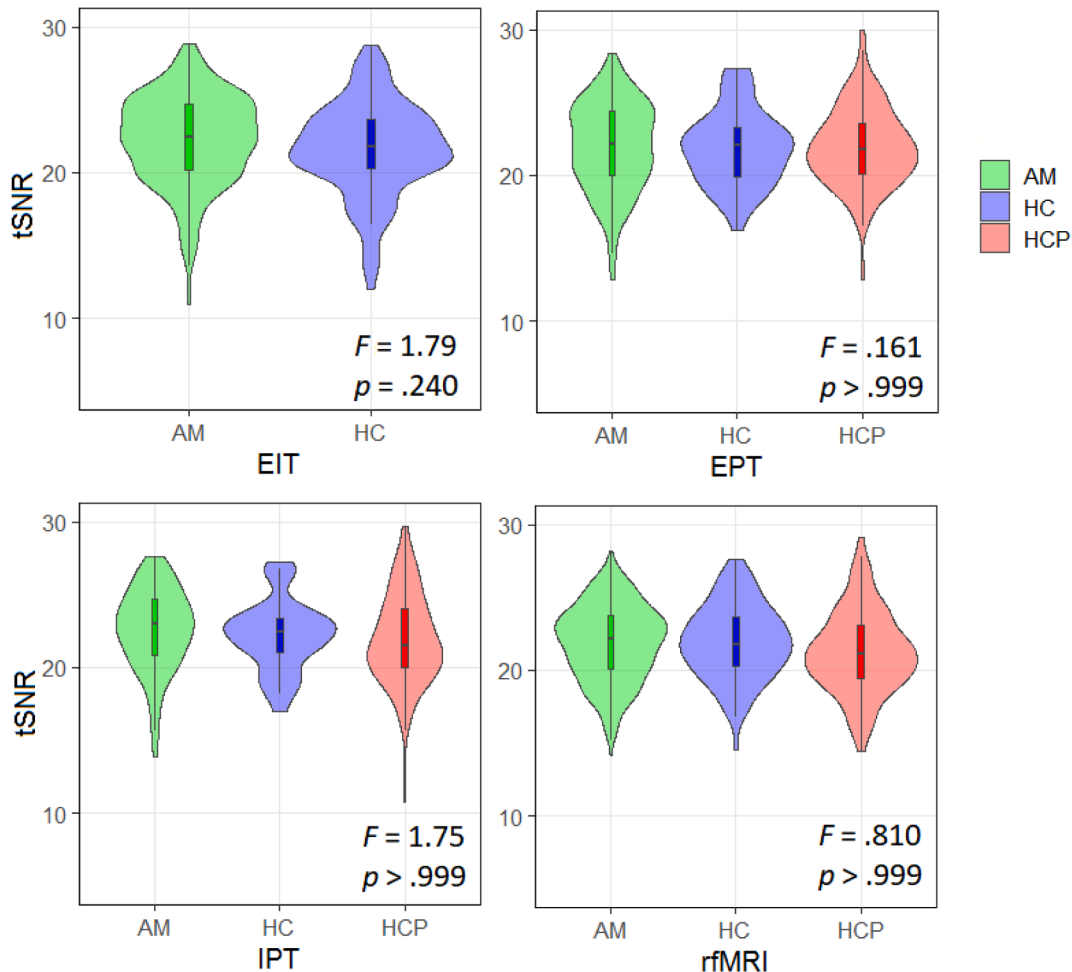
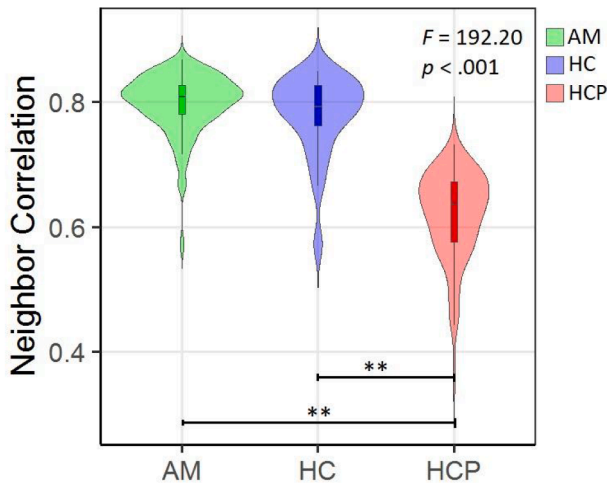


Fig. 8. Top row: temporal signal-to-noise ratio (tSNR) for Emotional Interference Task (EIT) and Emotional Processing Task (EPT); bottom row: tSNR for Incentive Processing Task (IPT) and resting state fMRI (rfMRI). AM = anxious misery (n = 97), HC = healthy control (n = 24), HCP = Human Connectome Project (n = 97). No significant group differences were observed. F-values and significance reported.

Differences in image quality and results can also be explained in part due to differences in sample; our subjects cover a wider range of ages than those present in the 1200 subject release of HCP-YA, and while we attempted to match across samples in age and controlled for age and sex

in our quantitative comparisons of image quality, our data still extend beyond the 36 years of age cutoff present in the HCP-YA release. Once the HCP-Aging dataset is fully released through the NIH-NDA, we will conduct further comparisons between our imaging data and data



**Fig. 9.** Neighbor correlation for diffusion weighted scans. AM = anxious misery (n = 97), HC = healthy control (n = 24), HCP = Human Connectome Project (n = 97). \*\* = significant at  $p < .001$ .

collected across the ongoing HCP Lifespan Studies.

Finally, differences reported in SNR and results may also be attributed to hardware differences between HCP-YA collection and our own. Notably, the Siemens Skyra platform in use at WashU is custom-built for the purpose of HCP acquisition and uses a 32-channel head coil, while all of our scans were collected on a Siemens Prisma 3 T system utilizing a 64-channel head coil. The Siemens Prisma (80 mT/m gradients for diffusion and ~ 42 mT/m gradient for imaging) has gradients similar to the custom Skyra system (100 mT/m gradients for diffusion and ~ 42 mT/m gradient for imaging), allowing for an exact duplication of structural and functional protocols in relation to TE and resolution;

diffusion encoding is necessarily different in our own protocol due to the difference in maximal gradient strength between Skyra and Prisma systems. For functional imaging, HCP recommends a multiband (MB) factor of 6 to 8 and a resolution of 2.0–2.5 mm, depending on the specifics of the system in use. In our functional imaging, we matched the recommended MB of 8 with a resolution of 2.0 mm in an attempt to obtain data of similar quality to HCP (Snyder, 2013). Due to the differences in each system, even identical parameters can yield different results across time, and we performed regular checks of temporal stability throughout data collection.

We also observed generally higher measures of cortical thickness (although relative distributions across the brain share similar features) and GFA (although trajectories across tracts appear similar) in our sample compared to the HCP-YA data. In addition to the possible sources listed above, these differences may be attributable to the as-of-yet unidentified effects of NVS pathology on the brain, although we reserve rigorous hypothesis testing to analyses that are outside of the scope of this report.

### 6.2. Comparison to HCP-YA neuropsychological and behavioral measures

In addition to the standard measures of the HCP, this project expanded its scope by implementing measures aimed at characterizing the behavioral and cognitive facets of anxious misery. Supplemental Table 7 gives a comprehensive comparison of the instruments used in this project compared with the ones in the HCP (Barch et al., 2013).

While this project employed the foundational measures of the HCP, such as the NIH Toolbox Cognitive and Emotional Batteries and Penn CNB, it did not implement measurements for motor, sensory or visual functioning, instead implementing two self-report surveys to measure physical functioning. Further, our project implemented additional clinician-administered and self-report measurements to assess the NVS constructs of loss and response to sustained threat. Specifically,

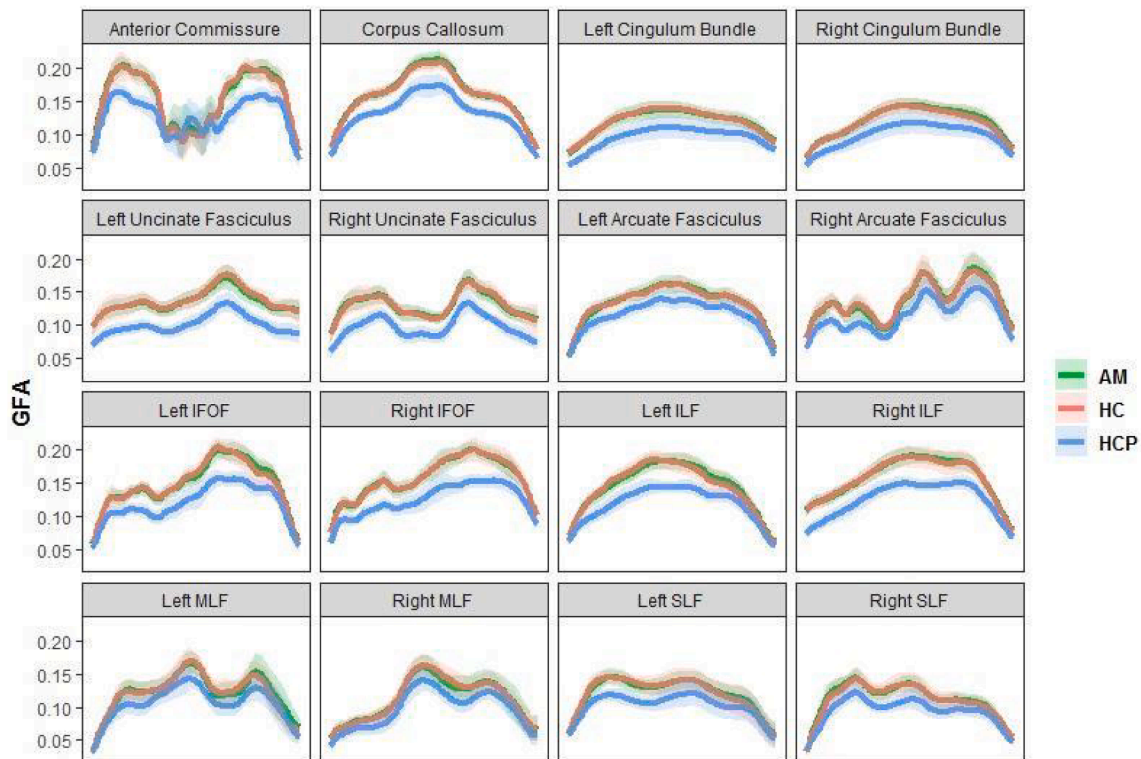


**Fig. 10.** Profiles of generalized fractional anisotropy (GFA) for 16 standard tracts. Group means are plotted, with shaded areas denoting standard deviation. X-axis indicates position along the tract. IFOF = inferior fronto occipital fasciculus, ILF = inferior lateral fasciculus, MLF = middle lateral fasciculus, SLF = superior lateral fasciculus, AM = anxious misery, HC = healthy control, HCP = Human Connectome Project.

clinician-administered measures including the Montgomery-Asberg Depression Rating Scale (MADRS) and the Hamilton Rating Scale for Depression (HAM-D) were used to evaluate depression severity, and the Columbia Suicide Severity Rating Scale was used to assess suicidal ideation. Self-report measures including the Anxiety Sensitivity Index (ASI), the Snaith-Hamilton Pleasure Scale (SHAPS) and the Ruminative Thought Scale (RTS) were administered to gather additional information regarding participants' depressive and anxious moods and behaviors. Additionally, this project implemented several measures measuring trauma in childhood, including the Childhood Trauma Questionnaire (CTQ) and the Maltreatment and Abuse Chronology of Exposure (MACE), as well as life stressors, including the Perceived Stress Scale (PSS), Life Events Stress (LES) Scale and Holmes-Rahe Life Stress Inventory (LSI).

### 6.3. Dimensional perspective

Designed to align with the NIMH RDoC framework, the Anxious Misery study has collected a comprehensive set of cognitive and behavioral measurements paired with state-of-the-art neuroimaging acquisitions. Importantly, our sample of participants has a heterogeneous mix of depressive, anxious and trauma related symptomology, making it an ideal dataset to examine transdiagnostic associations between elements of the Negative Valence domain of the RDoC matrix and neural circuit abnormalities as measured by MRI. As such, investigators are encouraged to adopt such a dimensional approach in their analyses of this dataset and seek to relate specific cognitive, behavioral and phenomenological elements with brain circuits.

Dimensional approaches can still benefit from a sample of healthy comparators. For example, when harmonizing neuroimaging data from multiple scanners, care must be taken to account for site- and scanner-related effects, as significant scanner effects can still be detected even when imaging protocols and scanning parameters are standardized (Noble et al., 2017). Methods like ComBat, which utilizes an empirical Bayes framework to improve the estimation of scanner effects, have proven successful in accounting for scanner-related variance of functional connectivity matrices, diffusion imaging metrics and cortical thickness (Fortin et al., 2018, 2017; Yu et al., 2018). However, estimation of scanner-related variance may be confounded by the effects of psychopathology, particularly when merging with a dataset of primarily healthy participants, like the HCP-YA dataset. Therefore, when aggregating the Anxious Misery cohort with datasets comprising exclusively healthy participants, we recommend that models of scanner effects be fit using our sample of healthy comparators and subsequently applied to our anxious misery participants in order to minimize these confounding effects. Examples of other uses of our sample of healthy comparators include methods like normative modeling, which can leverage techniques such as Gaussian process regression to model healthy brain imaging data distributions and examine how individual patients deviate from these normative patterns (Marquand et al., 2019, 2016).

### 6.4. Medication use

Past and present medication use is known to affect neuroimaging signatures of psychopathology (Phillips et al., 2008; Savitz et al., 2010; Smith et al., 2013). We did not require participants to have a washout period of current psychotropic medication, although the majority of participants (73.2%) were unmedicated at the time of enrollment. One potential limitation of the current project is the confounding effect of medication on neuroimaging measures in our medicated participants. To address this limitation, we collected extensive records of past and current medication use in order to account for medication-related effects on neuroimaging variables. Further, the inclusion of medicated individuals may also be a strength, as it improves the generalizability of our results to a wider population, as well as offers the opportunity to directly examine the effect of medication on neuroimaging data by

analyzing medicated and unmedicated participants separately.

### 6.5. Future directions

The current project is part of a larger series of studies within the HCP framework known collectively as the Human Connectome Studies Related to Human Disease (CRHD) and will contribute to building a database for comparisons between diverse populations. In particular, three other projects studying similar aspects of human psychopathology were funded at approximately the same time as the Anxious Misery project: Connectomes Related to Anxiety & Depression (PIs: Whitfield-Gabrieli & Gabrieli; Northeastern University & Massachusetts Institute of Technology) (Hubbard, 2020; Siless, 2020), Mapping Connectomes for Disordered Mental States (PI: Williams, Stanford University) (Tozzi, 2020) and Perturbation of the Treatment of Resistant Depression Connectome by Fast-Acting Therapies (PIs: Espinoza, Narr, & Wang; University of California, Los Angeles) (Loureiro et al., 2020; Vasavada et al., 2020). Respectively focusing on adolescents, patients experiencing emotional dysregulation and treatment-resistant patients, each of these projects has slightly different goals and patient populations.

The data collected in the present study will be harmonized with data from these three other studies of human psychopathology. This will require careful harmonization of imaging data to remove site and scanner-related effects, which, as we have previously described (Yu et al., 2018), is critical for the interpretability and validity of any results. In addition, the varied behavioral assessments implemented by each site will require careful attention to ensure that similar domains of psychopathology are captured in any metrics of patient variability (see Supplementary Table 8 for an overview of overlapping behavioral measures). Despite these challenges, concordance of scanning parameters and overlapping behavioral tasks with these three other CRHD projects enhances the viability of such a harmonization, which will ultimately result in a comprehensive database of brain and behavior data for over 800 participants across a wide range of age, disease-type and geographic locations.

## 7. Conclusion

The HCP study "Dimensional Connectomics of Anxious Misery" combines well-validated measures of psychopathology, emotion, and neurocognitive function with HCP-standard neuroimaging acquisitions. Measures of image quality indicate superior quality of structural acquisitions and equivalent quality of functional acquisitions to the HCP-YA sample. The availability of multimodal imaging together with behavioral and neurocognitive data will spur research on the relationships between dimensions of behavior and neuroimaging features, supporting Strategy 1.4 of the NIMH Strategic Plan: "Develop new ways of classifying disorders based on dimensions of observable behaviors and brain functions." The Anxious Misery dataset contributes to a new, dimensional description of psychopathology that is grounded in neuroscience and aims to capitalize on novel, circuit-based associations with measures of behavioral dimensions and neuropsychological dysfunction. Data will be made publicly available through the Connectome Coordinating Facility. The first half of the dataset (n = 121) will be available upon the initial public release to the NIH-NDA in fall 2020, with the remaining half of the dataset available in 2021.

### Disclosures

Dr. Shinohara receives personal compensation for reviewership duties for the American Medical Association and the Emerson Collective.

### Funding

This work was supported by the National Institute of Mental Health (U01 MH109991).

## CRediT authorship contribution statement

**Darsol Seok:** Methodology, Software, Formal analysis, Investigation, Data curation, Writing - original draft, Visualization. **Nathan Smyk:** Methodology, Data curation, Writing - original draft, Visualization. **Marc Jaskir:** Methodology, Data curation, Writing - original draft, Visualization. **Philip Cook:** Conceptualization, Methodology, Writing - review & editing. **Mark Elliott:** Conceptualization, Methodology, Writing - review & editing. **Tommaso Girelli:** Investigation, Writing - review & editing, Visualization. **J.Cobb Scott:** Conceptualization, Writing - review & editing. **Nicholas Balderston:** Writing - review & editing. **Joanne Beer:** Methodology, Writing - review & editing. **Janet Stock:** Investigation, Data curation, Supervision. **Walid Makhoul:** Investigation, Data curation. **Ruben Gur:** Conceptualization, Writing - review & editing. **Christos Davatzikos:** Conceptualization, Resources, Writing - review & editing. **Russell Shinohara:** Conceptualization, Methodology, Writing - review & editing. **Yvette Sheline:** Conceptualization, Writing - original draft, Writing - review & editing, Supervision, Project administration, Funding acquisition.

## Declaration of Competing Interest

The authors declare that they have no known competing financial interests or personal relationships that could have appeared to influence the work reported in this paper.

## Acknowledgements

The authors would like to thank Maria Prociuk for her expertise and assistance in submitting the manuscript. We would also like to thank the participants for their time and effort.

## Appendix A. Supplementary data

Supplementary data to this article can be found online at <https://doi.org/10.1016/j.nicl.2020.102489>.

## References

- Krueger, R.F., 1999. The Structure of Common Mental Disorders. *Arch Gen Psychiatry* 56 (10), 921. <https://doi.org/10.1001/archpsyc.56.10.921>.
- Watson, D., Rethinking the mood and anxiety disorders: a quantitative hierarchical model for DSM-V. *J Abnorm Psychol*, 2005. 114(4): p. 522-36.
- Watson, D., 2009. Differentiating the Mood and Anxiety Disorders: A Quadripartite Model. *Annu. Rev. Clin. Psychol.* 5 (1), 221–247. <https://doi.org/10.1146/annurev.clinpsy.032408.153510>.
- Insel, T.R., 2014. The NIMH Research Domain Criteria (RDoC) Project: Precision Medicine for Psychiatry. *AJP* 171 (4), 395–397. <https://doi.org/10.1176/appi.ajp.2014.14020138>.
- Bressler, S.L., Menon, V., 2010. Large-scale brain networks in cognition: emerging methods and principles. *Trends Cogn. Sci.* 14 (6), 277–290. <https://doi.org/10.1016/j.tics.2010.04.004>.
- Friston, K.J., 1996. Theoretical neurobiology and schizophrenia. *Br. Med. Bull.* 52 (3), 644–655. <https://doi.org/10.1093/oxfordjournals.bmb.a011573>.
- Van Essen, D.C., Smith, S.M., Barch, D.M., Behrens, T.E.J., Yacoub, E., Ugurbil, K., 2013. The WU-Minn Human Connectome Project: An overview. *NeuroImage* 80, 62–79. <https://doi.org/10.1016/j.neuroimage.2013.05.041>.
- Van Horn, J.D., Toga, A.W., 2009. Is it time to re-prioritize neuroimaging databases and digital repositories? *NeuroImage* 47 (4), 1720–1734.
- Bookheimer, S.Y., Salat, D.H., Terpstra, M., Ances, B.M., Barch, D.M., Buckner, R.L., Burgess, G.C., Curtiss, S.W., Diaz-Santos, M., Elam, J.S., Fischl, B., Greve, D.N., Hagy, H.A., Harms, M.P., Hatch, O.M., Hedden, T., Hodge, C., Japardi, K.C., Kuhn, T. P., Ly, T.K., Smith, S.M., Somerville, L.H., Ugurbil, K., van der Kouwe, A., Van Essen, D., Woods, R.P., Yacoub, E., 2019. The Lifespan Human Connectome Project in Aging: An overview. *NeuroImage* 185, 335–348. <https://doi.org/10.1016/j.neuroimage.2018.10.009>.
- LeWinn, K.Z., Sheridan, M.A., Keyes, K.M., Hamilton, A., McLaughlin, K.A., 2017. Sample composition alters associations between age and brain structure. *Nat. Commun.* 8 (1) <https://doi.org/10.1038/s41467-017-00908-7>.
- Cyranowski, J.M., Frank, E., Young, E., Shear, M.K., 2000. Adolescent Onset of the Gender Difference in Lifetime Rates of Major Depression: A Theoretical Model. *Arch Gen Psychiatry* 57 (1), 21. <https://doi.org/10.1001/archpsyc.57.1.21>.
- McCrae, R.R., Costa, P.T., Jr., 2007. Brief versions of the NEO-PI-3. *Journal of Individual Differences* 29 (3), 116–128.
- Andrews, G., Stewart, G., Morris-Yates, A., Holt, P., Henderson, S., 1990. Evidence for a General Neurotic Syndrome. *Br J Psychiatry* 157 (1), 6–12. <https://doi.org/10.1192/bjp.157.1.6>.
- Khan, A.A., Jacobson, K.C., Gardner, C.O., Prescott, C.A., Kendler, K.S., 2005. Personality and comorbidity of common psychiatric disorders. *Br J Psychiatry* 186 (3), 190–196. <https://doi.org/10.1192/bjp.186.3.190>.
- Gershon, R.C., Wagster, M.V., Hendrie, H.C., Fox, N.A., Cook, K.F., Nowinski, C.J., 2013. NIH Toolbox for Assessment of Neurological and Behavioral Function. *Neurology* 80 (Issue 11, Supplement 3), S2–S6. <https://doi.org/10.1212/WNL.0b013e3182872e5f>.
- Mungas, D., Heaton, R.A., Tulskey, D., Zelazo, P.D., Slotkin, J., Blitz, D., Lai, J.-S., Gershon, R., 2014. Factor Structure, Convergent Validity, and Discriminant Validity of the NIH Toolbox Cognitive Health Battery (NIHTB-CHB) in Adults. *J Int Neuropsychol Soc* 20 (6), 579–587. <https://doi.org/10.1017/S1355617714000307>.
- Snaith, R.P., Hamilton, M., Morley, S., Humayan, A., Hargreaves, D., Trigwell, P., 1995. A Scale for the Assessment of Hedonic Tone the Snaith–Hamilton Pleasure Scale. *Br J Psychiatry* 167 (1), 99–103. <https://doi.org/10.1192/bjp.167.1.99>.
- Taylor, S., et al., Robust dimensions of anxiety sensitivity: development and initial validation of the Anxiety Sensitivity Index-3. *Psychol Assess*, 2007. 19(2): p. 176–88.
- Reiss, S., Peterson, R.A., Gursky, D.M., McNally, R.J., 1986. Anxiety sensitivity, anxiety frequency and the prediction of fearfulness. *Behav. Res. Ther.* 24 (1), 1–8. [https://doi.org/10.1016/0005-7967\(86\)90143-9](https://doi.org/10.1016/0005-7967(86)90143-9).
- Pilkonis, P.A., et al., 2011. Item banks for measuring emotional distress from the Patient-Reported Outcomes Measurement Information System (PROMIS(R)): depression, anxiety, and anger. *Assessment* 18 (3), 263–283.
- Bastien, C.H., Vallieres, A., Morin, C.M., 2001. Validation of the Insomnia Severity Index as an outcome measure for insomnia research. *Sleep Med* 2 (4), 297–307.
- Carver, C.S. and T.L. White, Behavioral inhibition, behavioral activation and affective responses to impending reward and punishment: the BIS/BAS scales. *Journal of Personality and Social Psychology*, 1994. 67: p. 319–333.
- Nolen-Hoeksema, S., J. Morrow, and B.L. Fredrickson, Response styles and the duration of episodes of depressed mood. *J Abnorm Psychol*, 1993. 102(1): p. 20–8.
- Bernstein, D.P., et al., 1994. Initial reliability and validity of a new retrospective measure of child abuse and neglect. *Am. J. Psychiatry* 151 (8), 1132–1136.
- Noone, P.A., The Holmes-Rahe Stress Inventory. *Occup Med (Lond)*, 2017. 67(7): p. 581–582.
- Blanchard, E.B., Jones-Alexander, J., Buckley, T.C., Forneris, C.A., 1996. Psychometric properties of the PTSD checklist (PCL). *Behav. Res. Ther.* 34 (8), 669–673. [https://doi.org/10.1016/0005-7967\(96\)00033-2](https://doi.org/10.1016/0005-7967(96)00033-2).
- Michalos, A.C., Kahlke, M., 2014. Life events checklist. *PsycTESTS Dataset*.
- Ware Jr, J., Kosinski, M., Keller, S.D., 1996. A 12-Item Short-Form Health Survey: Construction of Scales and Preliminary Tests of Reliability and Validity. *Med. Care* 34 (3), 220–233. <https://doi.org/10.1097/00005650-199603000-00003>.
- Sheehan, D.V., Harnett-Sheehan, K., Raj, B.A., 1996. The measurement of disability. *Int. Clin. Psychopharmacol.* 11 (Supplement 3), 89–95. <https://doi.org/10.1097/00004850-199606003-00015>.
- Kertzman, S., Aladjem, Z., Milo, R., Ben-Nahum, Z., Birger, M., Grinspan, H., Weizman, A., Kotler, M., 2004. The utility of the Visual Analogue Scale for the assessment of depressive mood in cognitively impaired patients. *Int. J. Geriatr. Psychiatry* 19 (8), 789–796. <https://doi.org/10.1002/gps.1141>.
- Heatherton, T.F., et al., 1991. The Fagerstrom Test for Nicotine Dependence: a revision of the Fagerstrom Tolerance Questionnaire. *Addiction* 86 (9), 1119–1127. <https://doi.org/10.1111/j.1360-0443.1991.tb01879.x>.
- Weissman, M.M., Bothwell, S., 1976. Assessment of social adjustment by patient self-report. *Arch Gen Psychiatry* 33 (9), 1111–1115.
- Marks, I.M., Mathews, A.M., 1979. Brief standard self-rating for phobic patients. *Behav. Res. Ther.* 17 (3), 263–267. [https://doi.org/10.1016/0005-7967\(79\)90041-X](https://doi.org/10.1016/0005-7967(79)90041-X).
- Montgomery, S.A., Åsberg, M., 1979. A New Depression Scale Designed to be Sensitive to Change. *Br J Psychiatry* 134 (4), 382–389. <https://doi.org/10.1192/bjp.134.4.382>.
- Hamilton, M., 1960. A rating scale for depression. *J. Neurol. Neurosurg. Psychiatry* 23 (1), 56–62. <https://doi.org/10.1136/jnnp.23.1.56>.
- Posner, K., 2016. Columbia-Suicide Severity Rating Scale. *PsycTESTS Dataset*.
- Gur, R.C., et al., 2001. Computerized neurocognitive scanning: I. Methodology and validation in healthy people. *Neuropsychopharmacology* 25 (5), 766–776.
- Gur, R.C., et al., A cognitive neuroscience-based computerized battery for efficient measurement of individual differences: standardization and initial construct validation. *J Neurosci Methods*, 2010. 187(2): p. 254–62.
- Moore, T.M., et al., Psychometric properties of the Penn Computerized Neurocognitive Battery. *Neuropsychology*, 2015. 29(2): p. 235–46.
- Etkin, A., A. Gyurak, and R. O'Hara, A neurobiological approach to the cognitive deficits of psychiatric disorders. *Dialogues Clin Neurosci*, 2013. 15(4): p. 419–29.
- Scott, J.C., et al., A quantitative meta-analysis of neurocognitive functioning in posttraumatic stress disorder. *Psychol Bull*, 2015. 141(1): p. 105–140.
- Snyder, H.R., 2013. Major depressive disorder is associated with broad impairments on neuropsychological measures of executive function: a meta-analysis and review. *Psychol Bull* 139 (1), 81–132.
- Yushkevich, P.A., Wang, H., Pluta, J., Das, S.R., Craige, C., Avants, B.B., Weiner, M.W., Mueller, S., 2010. Nearly automatic segmentation of hippocampal subfields in in vivo focal T2-weighted MRI. *NeuroImage* 53 (4), 1208–1224. <https://doi.org/10.1016/j.neuroimage.2010.06.040>.
- Fales, C.L., Barch, D.M., Rundle, M.M., Mintun, M.A., Snyder, A.Z., Cohen, J.D., Mathews, J., Sheline, Y.L., 2008. Altered Emotional Interference Processing in Affective and Cognitive-Control Brain Circuitry in Major Depression. *Biol. Psychiatry* 63 (4), 377–384. <https://doi.org/10.1016/j.biopsych.2007.06.012>.
- Vuilleumier, P., Armony, J.L., Driver, J., Dolan, R.J., 2001. Effects of Attention and Emotion on Face Processing in the Human Brain. *Neuron* 30 (3), 829–841. [https://doi.org/10.1016/S0896-6273\(01\)00328-2](https://doi.org/10.1016/S0896-6273(01)00328-2).

- Hariri, A.R., Tessitore, A., Mattay, V.S., Fera, F., Weinberger, D.R., 2002. The Amygdala Response to Emotional Stimuli: A Comparison of Faces and Scenes. *NeuroImage* 17 (1), 317–323. <https://doi.org/10.1006/nimg.2002.1179>.
- Delgado, M.R., Nystrom, L.E., Fissell, C., Noll, D.C., Fiez, J.A., 2000. Tracking the Hemodynamic Responses to Reward and Punishment in the Striatum. *J. Neurophysiol.* 84 (6), 3072–3077. <https://doi.org/10.1152/jn.2000.84.6.3072>.
- Glasser, M.F., Sotiropoulos, S.N., Wilson, J.A., Coalson, T.S., Fischl, B., Andersson, J.L., Xu, J., Jbabdi, S., Webster, M., Polimeni, J.R., Van Essen, D.C., Jenkinson, M., 2013. The minimal preprocessing pipelines for the Human Connectome Project. *NeuroImage* 80, 105–124. <https://doi.org/10.1016/j.neuroimage.2013.04.127>.
- Esteban, O., Markiewicz, C.J., Blair, R.W., Moodie, C.A., Isik, A.I., Erramuzpe, A., Kent, J. D., Goncalves, M., DuPre, E., Snyder, M., Oya, H., Ghosh, S.S., Wright, J., Durnez, J., Poldrack, R.A., Gorgolewski, K.J., 2019. fMRIPrep: a robust preprocessing pipeline for functional MRI. *Nat Methods* 16 (1), 111–116. <https://doi.org/10.1038/s41592-018-0235-4>.
- Gorgolewski, K., et al., 2011. Nipype: a flexible, lightweight and extensible neuroimaging data processing framework in python. *Front Neuroinform* 5, 13.
- Tustison, N.J., Avants, B.B., Cook, P.A., Yuanjie Zheng, Egan, A., Yushkevich, P.A., Gee, J.C., 2010. N4ITK: Improved N3 Bias Correction. *IEEE Trans. Med. Imaging* 29 (6), 1310–1320. <https://doi.org/10.1109/TMI.2010.2046908>.
- Fonov, V.S., Evans, A.C., McKinstry, R.C., Almlri, CR, Collins, D.L., 2009. Unbiased nonlinear average age-appropriate brain templates from birth to adulthood. *NeuroImage* 47, S102. [https://doi.org/10.1016/S1053-8119\(09\)70884-5](https://doi.org/10.1016/S1053-8119(09)70884-5).
- Avants, B., Epstein, C., Grossman, M., Gee, J., 2008. Symmetric diffeomorphic image registration with cross-correlation: Evaluating automated labeling of elderly and neurodegenerative brain. *Med. Image Anal.* 12 (1), 26–41. <https://doi.org/10.1016/j.media.2007.06.004>.
- Zhang, Y., M. Brady, and S. Smith, Segmentation of brain MR images through a hidden Markov random field model and the expectation-maximization algorithm. *IEEE Trans Med Imaging*, 2001. 20(1): p. 45-57.
- Jenkinson, M., Bannister, P., Brady, M., Smith, S., 2002. Improved Optimization for the Robust and Accurate Linear Registration and Motion Correction of Brain Images. *NeuroImage* 17 (2), 825–841. <https://doi.org/10.1006/nimg.2002.1132>.
- Andersson, J.L.R., Skare, S., Ashburner, J., 2003. How to correct susceptibility distortions in spin-echo echo-planar images: application to diffusion tensor imaging. *NeuroImage* 20 (2), 870–888. [https://doi.org/10.1016/S1053-8119\(03\)00336-7](https://doi.org/10.1016/S1053-8119(03)00336-7).
- Cox, R.W., 1996. AFNI: Software for Analysis and Visualization of Functional Magnetic Resonance Neuroimages. *Comput. Biomed. Res.* 29 (3), 162–173. <https://doi.org/10.1006/cbmr.1996.0014>.
- Greve, D.N., Fischl, B., 2009. Accurate and robust brain image alignment using boundary-based registration. *NeuroImage* 48 (1), 63–72. <https://doi.org/10.1016/j.neuroimage.2009.06.060>.
- Behzadi, Y., Restom, K., Liu, J., Liu, T.T., 2007. A component based noise correction method (CompCor) for BOLD and perfusion based fMRI. *NeuroImage* 37 (1), 90–101. <https://doi.org/10.1016/j.neuroimage.2007.04.042>.
- Power, J.D., Mitra, A., Laumann, T.O., Snyder, A.Z., Schlaggar, B.L., Petersen, S.E., 2014. Methods to detect, characterize, and remove motion artifact in resting state fMRI. *NeuroImage* 84, 320–341. <https://doi.org/10.1016/j.neuroimage.2013.08.048>.
- Abraham, A., et al., 2014. Machine learning for neuroimaging with scikit-learn. *Front Neuroinform* 8, 14.
- Ciric, R., Rosen, A.F.G., Erus, G., Cieslak, M., Adebimpe, A., Cook, P.A., Bassett, D.S., Davatzikos, C., Wolf, D.H., Satterthwaite, T.D., 2018. Mitigating head motion artifact in functional connectivity MRI. *Nat Protoc* 13 (12), 2801–2826. <https://doi.org/10.1038/s41596-018-0065-y>.
- Biswal, B.B., Mennes, M., Zuo, X.-N., Gohel, S., Kelly, C., Smith, S.M., Beckmann, C.F., Adelstein, J.S., Buckner, R.L., Colcombe, S., Dogonowski, A.-M., Ernst, M., Fair, D., Hampson, M., Hoptman, M.J., Hyde, J.S., Kiviniemi, V.J., Kottler, R., Li, S.-J., Lin, C.-P., Lowe, M.J., Mackay, C., Madden, D.J., Madsen, K.H., Margulies, D.S., Mayberg, H.S., McMahon, K., Monk, C.S., Mostofsky, S.H., Nagel, B.J., Pekar, J.J., Peltier, S.J., Petersen, S.E., Riedel, V., Rombouts, S.A.R.B., Rypma, B., Schlaggar, B.L., Schmidt, S., Seidler, R.D., Siegle, G.J., Sorg, C., Teng, G.-J., Veijola, J., Villringer, A., Walter, M., Wang, L., Weng, X.-C., Whitfield-Gabrieli, S., Williamson, P., Windischberger, C., Zang, Y.-F., Zhang, H.-Y., Castellanos, F.X., Milham, M.P., 2010. Toward discovery science of human brain function. *Proc. Natl. Acad. Sci.* 107 (10), 4734–4739. <https://doi.org/10.1073/pnas.0911855107>.
- Satterthwaite, T.D., Elliott, M.A., Gerraty, R.T., Ruparel, K., Loughhead, J., Calkins, M.E., Eickhoff, S.B., Hakonarson, H., Gur, R.C., Gur, R.E., Wolf, D.H., 2013. An improved framework for confound regression and filtering for control of motion artifact in the preprocessing of resting-state functional connectivity data. *NeuroImage* 64, 240–256. <https://doi.org/10.1016/j.neuroimage.2012.08.052>.
- Smith, S.M., Brady, J.M., 1997. SUSAN-A new approach to low level image processing. *Int. J. Comput. Vision* 23, 45–78.
- Smith, S.M., Jenkinson, M., Woolrich, M.W., Beckmann, C.F., Behrens, T.E.J., Johansen-Berg, H., Bannister, P.R., De Luca, M., Drobnjak, I., Flitney, D.E., Niazy, R.K., Saunders, J., Vickers, J., Zhang, Y., De Stefano, N., Brady, J.M., Matthews, P.M., 2004. Advances in functional and structural MR image analysis and implementation as FSL. *NeuroImage* 23, S208–S219. <https://doi.org/10.1016/j.neuroimage.2004.07.051>.
- Smith, S.M., Hyvärinen, A., Varoquaux, G., Miller, K.L., Beckmann, C.F., 2014. Group-PCA for very large fMRI datasets. *NeuroImage* 101, 738–749. <https://doi.org/10.1016/j.neuroimage.2014.07.051>.
- Sotiropoulos, S.N., Jbabdi, S., Xu, J., Andersson, J.L., Moeller, S., Auerbach, E.J., Glasser, M.F., Hernandez, M., Sapiro, G., Jenkinson, M., Feinberg, D.A., Yacoub, E., Lenglet, C., Van Essen, D.C., Ugurbil, K., Behrens, T.E.J., 2013. Advances in diffusion MRI acquisition and processing in the Human Connectome Project. *NeuroImage* 80, 125–143. <https://doi.org/10.1016/j.neuroimage.2013.05.057>.
- Avants, B.B., Tustison, N.J., Song, G., Cook, P.A., Klein, A., Gee, J.C., 2011. A reproducible evaluation of ANTs similarity metric performance in brain image registration. *NeuroImage* 54 (3), 2033–2044. <https://doi.org/10.1016/j.neuroimage.2010.09.025>.
- Yeh, F.C., et al., Deterministic diffusion fiber tracking improved by quantitative anisotropy. *PLoS One*, 2013. 8(11): p. e80713.
- Yeh, F.-C., Panesar, S., Fernandes, D., Meola, A., Yoshino, M., Fernandez-Miranda, J.C., Vettel, J.M., Verstynen, T., 2018. Population-averaged atlas of the macroscale human structural connectome and its network topology. *NeuroImage* 178, 57–68. <https://doi.org/10.1016/j.neuroimage.2018.05.027>.
- Van Essen, D.C., Glasser, M.F., Dierker, D.L., Harwell, J., Coalson, T., 2012. Parcellations and Hemispheric Asymmetries of Human Cerebral Cortex Analyzed on Surface-Based Atlases. *Cereb. Cortex* 22 (10), 2241–2262. <https://doi.org/10.1093/cercor/bhr291>.
- Yeh, F.C., et al., 2019. Differential tractography as a track-based biomarker for neuronal injury. *NeuroImage* 202, 116131.
- Roalf, D.R., Quarmley, M., Elliott, M.A., Satterthwaite, T.D., Vandekar, S.N., Ruparel, K., Gennatas, E.D., Calkins, M.E., Moore, T.M., Hopson, R., Prabhakaran, K., Jackson, C. T., Verma, R., Hakonarson, H., Gur, R.C., Gur, R.E., 2016. The impact of quality assurance assessment on diffusion tensor imaging outcomes in a large-scale population-based cohort. *NeuroImage* 125, 903–919. <https://doi.org/10.1016/j.neuroimage.2015.10.068>.
- Satterthwaite, T.D., Wolf, D.H., Loughhead, J., Ruparel, K., Elliott, M.A., Hakonarson, H., Gur, R.C., Gur, R.E., 2012. Impact of in-scanner head motion on multiple measures of functional connectivity: Relevance for studies of neurodevelopment in youth. *NeuroImage* 60 (1), 623–632. <https://doi.org/10.1016/j.neuroimage.2011.12.063>.
- Kanwisher, N., McDermott, J., Chun, M.M., 1997. The Fusiform Face Area: A Module in Human Extrastriate Cortex Specialized for Face Perception. *J. Neurosci.* 17 (11), 4302–4311. <https://doi.org/10.1523/JNEUROSCI.17-11-04302.1997>.
- Epstein, R., Kanwisher, N., 1998. A cortical representation of the local visual environment. *Nature* 392 (6676), 598–601. <https://doi.org/10.1038/33402>.
- Davachi, L., 2006. Item, context and relational episodic encoding in humans. *Curr. Opin. Neurobiol.* 16 (6), 693–700. <https://doi.org/10.1016/j.conb.2006.10.012>.
- O'Doherty, J., Kringelbach, M.L., Rolls, E.T., Hornak, J., Andrews, C., 2001. Abstract reward and punishment representations in the human orbitofrontal cortex. *Nat Neurosci* 4 (1), 95–102. <https://doi.org/10.1038/82959>.
- Raichle, M.E., MacLeod, A.M., Snyder, A.Z., Powers, W.J., Gusnard, D.A., Shulman, G.L., 2001. A default mode of brain function. *Proc. Natl. Acad. Sci.* 98 (2), 676–682. <https://doi.org/10.1073/pnas.98.2.676>.
- Fox, M.D., Corbetta, M., Snyder, A.Z., Vincent, J.L., Raichle, M.E., 2006. Spontaneous neuronal activity distinguishes human dorsal and ventral attention systems. *Proc. Natl. Acad. Sci.* 103 (26), 10046–10051. <https://doi.org/10.1073/pnas.0604187103>.
- Geyer, S., The microstructural border between the motor and the cognitive domain in the human cerebral cortex. *Adv Anat Embryol Cell Biol*, 2004. 174: p. I-VIII, 1-89.
- Barch, D.M., Burgess, G.C., Harms, M.P., Petersen, S.E., Schlaggar, B.L., Corbetta, M., Glasser, M.F., Curtiss, S., Dixit, S., Feldt, C., Nolan, D., Bryant, E., Hartley, T., Footer, O., Bjork, J.M., Poldrack, R., Smith, S., Johansen-Berg, H., Snyder, A.Z., Van Essen, D.C., 2013. Function in the human connectome: Task-fMRI and individual differences in behavior. *NeuroImage* 80, 169–189. <https://doi.org/10.1016/j.neuroimage.2013.05.033>.
- Noble, S., Scheinost, D., Finn, E.S., Shen, X., Papademetris, X., McEwen, S.C., Bearden, C. E., Addington, J., Goodyear, B., Cadenhead, K.S., Mirzakhani, H., Cornblatt, B.A., Olvet, D.M., Mathalon, D.H., McGlashan, T.H., Perkins, D.O., Belger, A., Seidman, L. J., Thermenos, H., Tsuang, M.T., van Erp, T.G.M., Walker, E.F., Hamann, S., Woods, S.W., Cannon, T.D., Constable, R.T., 2017. Multisite reliability of MR-based functional connectivity. *NeuroImage* 146, 959–970. <https://doi.org/10.1016/j.neuroimage.2016.10.020>.
- Fortin, J.-P., Cullen, N., Sheline, Y.I., Taylor, W.D., Aseelcioglu, I., Cook, P.A., Adams, P., Cooper, C., Fava, M., McGrath, P.J., McInnis, M., Phillips, M.L., Trivedi, M.H., Weissman, M.M., Shinohara, R.T., 2018. Harmonization of cortical thickness measurements across scanners and sites. *NeuroImage* 167, 104–120. <https://doi.org/10.1016/j.neuroimage.2017.11.024>.
- Fortin, J.-P., Parker, D., Tunç, B., Watanabe, T., Elliott, M.A., Ruparel, K., Roalf, D.R., Satterthwaite, T.D., Gur, R.C., Gur, R.E., Schultz, R.T., Verma, R., Shinohara, R.T., 2017. Harmonization of multi-site diffusion tensor imaging data. *NeuroImage* 161, 149–170. <https://doi.org/10.1016/j.neuroimage.2017.08.047>.
- Yu, M., Linn, K.A., Cook, P.A., Phillips, M.L., McInnis, M., Fava, M., Trivedi, M.H., Weissman, M.M., Shinohara, R.T., Sheline, Y.I., 2018. Statistical harmonization corrects site effects in functional connectivity measurements from multi-site fMRI data. *Hum Brain Mapp* 39 (11), 4213–4227. <https://doi.org/10.1002/hbm.24241>.
- Marquand, A.F., Kia, S.M., Zabihi, M., Wolfers, T., Buitelaar, J.K., Beckmann, C.F., 2019. Conceptualizing mental disorders as deviations from normative functioning. *Mol Psychiatry* 24 (10), 1415–1424. <https://doi.org/10.1038/s41380-019-0441-1>.
- Marquand, A.F., Rezek, I., Buitelaar, J., Beckmann, C.F., 2016. Understanding Heterogeneity in Clinical Cohorts Using Normative Models: Beyond Case-Control Studies. *Biol. Psychiatry* 80 (7), 552–561. <https://doi.org/10.1016/j.biopsych.2015.12.023>.
- Phillips M.D., M.L., Travis M.D., M.J., Fagioli M.D., A., Kupfer M.D., D.J., 2008. Medication Effects in Neuroimaging Studies of Bipolar Disorder. *AJP* 165 (3), 313–320. <https://doi.org/10.1176/appi.ajp.2007.0701066>.
- Savitz, J., Nugent, A.C., Bogers, W., Liu, A., Sills, R., Luckenbaugh, D.A., Bain, E.E., Price, J.L., Zarate, C., Manji, H.K., Cannon, D.M., Marrett, S., Charney, D.S., Drevets, W.C., 2010. Amygdala volume in depressed patients with bipolar disorder assessed with high resolution 3T MRI: The impact of medication. *NeuroImage* 49 (4), 2966–2976. <https://doi.org/10.1016/j.neuroimage.2009.11.025>.

- Smith, R., Chen, K., Baxter, L., Fort, C., Lane, R.D., 2013. Antidepressant effects of sertraline associated with volume increases in dorsolateral prefrontal cortex. *J. Affect. Disord.* 146 (3), 414–419. <https://doi.org/10.1016/j.jad.2012.07.029>.
- Hubbard, N.A., et al., 2020. Brain function and clinical characterization in the Boston adolescent neuroimaging of depression and anxiety study. *Neuroimage Clin.* 27, 102240.
- Siless, V., et al., 2020. Image acquisition and quality assurance in the Boston Adolescent Neuroimaging of Depression and Anxiety study. *Neuroimage Clin.* 26, 102242.
- Tozzi, L., et al., 2020. The human connectome project for disordered emotional states: Protocol and rationale for a research domain criteria study of brain connectivity in young adult anxiety and depression. *Neuroimage* 214, 116715.
- Loureiro, J.R.A., Leaver, A., Vasavada, M., Sahib, A.K., Kubicki, A., Joshi, S., Woods, R. P., Wade, B., Congdon, E., Espinoza, R., Narr, K.L., 2020. Modulation of amygdala reactivity following rapidly acting interventions for major depression. *Hum. Brain Mapp.* 41 (7), 1699–1710. <https://doi.org/10.1002/hbm.24895>.
- Vasavada, M.M., Loureiro, J., Kubicki, A., Sahib, A., Wade, B., Helleman, G., Espinoza, R.T., Congdon, E., Narr, K.L., Leaver, A.M., 2020. Effects of Serial Ketamine Infusions on Corticolimbic Functional Connectivity in Major Depression. *Biol. Psychiatry: Cogn. Neurosci. Neuroimaging.* <https://doi.org/10.1016/j.bpsc.2020.06.015>.